PRODUCTION OF ALUMINA BASED POROUS CERAMICS USING NAPHTHALENE AS THE PORE FORMER

A Thesis Submitted

In Partial Fulfillment of the Requirement

For the degree of

BACHELOR OF TECHNOLOGY

By

SOUMYA SURABHI

ROLL 108CR046

TO THE

DEPARTMENT OF CERAMIC ENGINEERING

NATIONAL INSTITUTE OF TECHNOLOGY ROURKELA

MAY 2012

CERTIFICATE

This is certified that the work contained in the project entitled "PRODUCTION OF ALUMINA BASED POROUS CERAMICS USING NAPHTHALENE AS THE PORE FORMER" by Soumya Surabhi (Roll 108CR046) in partial fulfillment of the requirements of the award of Bachelor of Technology Degree in Ceramic Engineering at the National Institute of Technology, Rourkela is an authentic work carried out by her under my supervision and guidance. To the best of my knowledge, the matter embodied in the thesis has not been submitted to any other university / institute for the award of any Degree or Diploma.

S.BHATTACHARYYA

PROFESSOR

Department of Ceramic Engineering

National Institute of Technology

Rourkela-769008

ACKNOWLEDGEMENT

I express my deep gratitude to my guide, Prof S. Bhattacharyya, Department of Ceramic Engineering, N I T Rourkela, for his valuable advice, time and guidance in the completion of this project work. My heartfelt thanks to all the faculty members for their suggestions during this project work. My sincere acknowledgement to the Research Scholars, M. Tech students and the non-teaching staff for the help and cooperation extended to us. And finally, my hearty thanks to all my friends who have constantly helped me.

Soumya Surabhi

108CR046

LIST OF FIGURES:

LIST OF TABLES:

CONTENTS

CHAPTER 3: EXPERIMENTAL WORK

CHAPTER 4: RESULTS & DISCUSSIONS

ABSTRACT

The present work focuses on the production of alumina based porous ceramics and its characterization. Five different alumina samples having naphthalene wt% between (0 -50) % were prepared by die pressing. Pellets were fired at different range of temperatures (1500 – 1600^{o}C) and time (2 – 4 hrs). It was found that with increase in the weight percentage (wt %) of naphthalene, the porosity increases. The pore size distribution also changes to larger pore sizes. CCS, bi-axial flexural strength decreases with increase in the porosity level and increases with the increase in sintering temperature and time. The strength vs porosity plots showed that the strength decreases exponentially with temperature and ln (CCS) vs porosity plots showed a linear fit with a negative slope. The SEM microstructure could describe briefly the distribution of the porosity inside those pellets and the average size of pores.

CHAPTER-1:

INTRODUCTION

1.1. *Introduction:*

Porous ceramics have become increasingly important in industry recently due to their numerous applications and utilizations involving different materials like metals, ceramics, polymers, composites, semiconductors and biomaterials.[1] Porosity can affect performance, properties, strength (both flexural and compressive), and density of materials. There has been a long tradition in producing porous materials, mainly for structural applications which include concrete, cements, bricks and refractories.[2] In all applications of porous material, transport through the pore phase is very important which can be achieved if the materials contain more than 10% connected porosity and pore volume. This type of porous ceramics finds key applications as supports for heterogeneous catalysts, membranes for bioreactors, environmental filters for hot flue gases and diesel engine emissions etc.

Porous ceramics are either reticulate (interconnected voids surrounded by a web of ceramic) or foam (closed voids within a continuous ceramic matrix).[3] These porous network structures have relatively low density, low mass and low thermal conductivity. Permeability is high in reticulate and low in foam ceramics due to the open-versus closed-cell structures, respectively.[4] Reticulate porous ceramics are commonly used for molten metal, diesel engine exhaust filters, catalyst supports and industrial hot-gas filters. Both reticulate and foam ceramics are utilized as light-structure plates, fire-protection materials and gas combustion burners. Porous ceramics are usually synthesized by either the polymeric-sponge method or by the foaming method.[4] Fig. 1.1 shows a picture of porous ceramics.

Fig. 1.1. Picture of Porous Ceramics [3]

Pore size control is the key factor in fabrication of porous materials. Particle size and size distribution of the raw materials, processing techniques, types of binder used, distribution of binder and sintering affect the final porosity and pore connectivity.[5]

Alumina is used for making porous ceramics because most of the alumina-based ceramics possess relatively high strength along with improved thermal and chemical stability.[6] Porous alumina materials are used in various forms, e.g. as polymeric foams for packaging and porous ceramics for water purification.[7] Because of their inherently brittle nature, pores have been traditionally avoided in ceramic components because pores reduce the material's strength. However, applications of porous ceramics have increased in the last decades, especially for environments where high temperatures, excessive wear and corrosive environment are involved.[8] Such applications include the filtration of molten metals, high-temperature thermal insulation, filtration of particulates from diesel engine exhaust gases, support for catalytic reactions, and filtration of hot corrosive gases in various industrial operations.[7-9] Porous ceramics are used in these applications due to the following advantages like high melting point, high corrosion resistance and wear resistance along with the features gained by the replacement

of solid material by voids in the material. Such features include low thermal mass, low thermal conductivity, controlled permeability, high surface area, low density, high specific strength, and low dielectric constant. These properties can be modified for each specific application by controlling the composition and microstructure of the porous ceramic.[9] Fluctuations in open and closed porosity, pore size distribution, and pore morphology can have a major effect on a material's properties. These microstructural features are in turn greatly influenced by the processing route used for the production of the porous material.

There are broadly two routes to fabricate three dimensional porous substrates, which vary according to the temperature applied.

(1) High temperature routes
    (a) Pyrolysis of organic particles[10]
    (b) Foam sintering[11]
    (c) Gel-casting[12]
    (d) Polymeric sponge technique[13]
    (e) Coextrusion process[14]
(2) Low Temperature Routes
    (a) Leaching[15]
    (b) Hydrothermal exchange[16]
    (c) Bicontinuous micro emulsion technique[17]

The choice of processing route for the production of a specific porous ceramics will depend on the final properties and applications aimed.

CHAPTER-2:

LITERATURE REVIEW

2.1. *Porous Ceramics and its Applications:*

Porous ceramics are nowadays being investigated for a variety of applications including molten metal and hot gas filters, light- weight structural components, electrodes, sensors, bioreactors, catalyst carriers, radiant burners and as porous implant in the area of biomaterials due to their specific properties like high surface area, high temperature stability, high permeability, low weight and low thermal conductivity.[18]

2.2. *Types of Porous Ceramics*

Porous ceramic products can be categorized according to the following specifications:[19]

- Chemical composition of raw material: alumino-silicate, silicate, oxide, non-oxide etc.
- Porosity: moderate (30-50%), high porosity (60-75%), and super-high porosity (over 75%)
- Physical state of products: continuous, filling, piecewise
- Inner structure: granular, cellular, fibrous
- Refractoriness correlated to service temperatures: low-melting (below 1350^{o}C), high-melting (1350-1580^{o}C), refractory (1580-1770^{o}C), highly refractory (1770-2000^{o}C), super refractory (over 2000^{o}C)
- Destination and application area: heat insulating (main parameter: thermal conductivity); heat shielding (main parameter: product of heat conductivity and apparent density values), and permeable (main parameters: porosity, pore size and permeability)

Porous ceramics can be generally divided into two categories: reticulate ceramics and foam ceramics. A reticulate ceramic consists of interconnected voids surrounded by a web of ceramic struts and is fabricated by infiltration and replication of a polymeric sponge perform. Infiltration of ceramic slurry and sintering yields an open porous ceramic structure, characterized by a hollow strut due to the burn out of the preform.[18] A ceramic foam consists of closed and open pores within a continuous ceramic matrix and is usually made by foaming processes applying foaming agents or by powder consolidation using fugitive organic additives as pore formers.[20] Both types of porous ceramics exhibit nearly isotropic pore morphology but differ in the porosity, size and shape of pores and permeability. Permeability is high in reticulate ceramics as compared to open or closed pore foam ceramics due to the larger pore size as well as open pore structure.

O. Lyckfeldt et al.[21] developed a new consolidation method for forming porous ceramics using starch as both consolidator/binder and pore former. Simple and complex-shaped components of porous alumina were shaped and demoulded in wet state. After drying, burn- out and sintering, materials with ultimate porosities between 23 and 70% were obtained.

2.3. ***Fabrication of Porous Ceramics***

The development of porous ceramic materials has presented a new challenge to several industries, because porous ceramics are more durable in extreme environments and their surface characteristics permit them to fulfill very specific requirements. With the growing demand for porous ceramics in industrial applications, a number of technologies have developed lately for fabricating these materials and their pore characteristics and to identify pore-related properties. A

tailor made porous ceramics can be made through a critical understanding and interpretation of the relationship, between various pore-related properties and optimizing them for specific uses. Presently, different porous ceramics with more delicate and uniform pore structures, having wide pore size range (few micrometers to a few nanometers) can be prepared for diverse purposes via varied physical and chemical processing.

R. Svinka et al.[22] studied the production of porous alumina ceramics by the slurry casting method and investigated pore formation by elimination of hydrogen as a result of a chemical reaction of aluminum powder with water. The purpose of study was to determine various ways of producing high porosity alumina ceramics having high mechanical strength and other properties significant for refractory ceramics.

To fulfill the requirement for bone tissue integration, the main morphological requirements for the porous substrates are the existence of open and interconnected pores, with pore diameters larger than 100 μm for proper vascularization.[23]

Kajutaka Kamitani et al.[24] fabricated highly porous alumina based ceramics by a slip casting method by employing polymethylmethacrylate (PMMA) microspheres having different diameters as a template and MgO/SiC powder as a sintering aid and subsequent calcinations at 1600^{o}C. The sintered product contained spherical pores relating to the morphology of PMMA microspheres. In addition, the formation of much smaller connected space among the pores was observed on the pore's inner walls of the ceramics. Highly porous and mechanically strong alumina ceramics having an open porosity of 62%, a connected space size of 1.3μm, and a compressive strength of 147.6 MPa could be fabricated by employing PMMA microspheres with a mean particle size of 22.6μm and an appropriate amount of MgO/SiC.

Various processing have been developed which have used replica, sacrificial template or direct foaming methods for the production of various porous ceramics. Fig. 2.1 provides a summary of the three basic schemed processing routes for the production of porous ceramics.

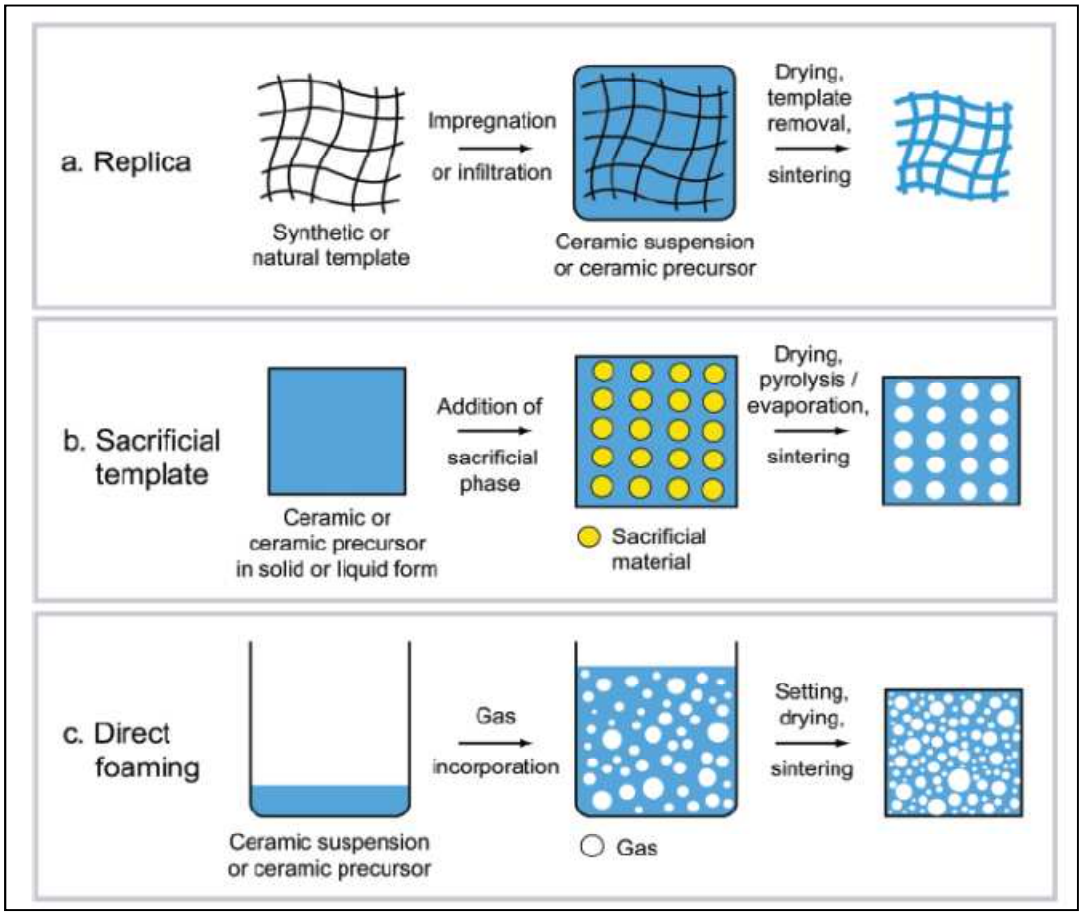

Fig. 2.1. Scheme of Possible Processing Routes of Porous Ceramics[9]

2.3.1. ***Replica Technique***[25-34]

The replica method involves the impregnation of a cellular structure with a ceramic suspension/precursor solution for the production of a porous ceramic showing the same

morphology as the original porous material.[25] Many natural and synthetic cellular structures are used as templates to fabricate porous ceramics through this technique.

(1) *Synthetic templates*[25-28]

Sponge replica technique is one of the best processing methods for porous ceramics and is used in industry to prepare ceramic filters for molten metal filtration and other useful applications. The polymer replica technique is a well-established method to prepare open cellular structures with pore sizes ranging from 200 mm to 3 mm at between 40% and 95% porosity.[25] The rheology of the impregnating suspension and its adhesion on the polymeric sponge are the most essential steps in this method. Due to high interconnectivity between pores, the permeability of fluids and gases is enhanced through the porous structure making these reticulated materials desirable for high through-put filtration.[26] Despite the easiness of this technique, the mechanical strength of cellular structures processed through this route can be considerably degraded by the formation of cracked struts during pyrolysis of the polymeric sponge.[27]

Miqin Zhang et al.[28] introduced a new technique by combining the gel-casting and polymer sponge methods to prepare macroporous hydroxyapatite scaffolds, which provides a more effective control over the microstructures of scaffolds and helps in enhancing their mechanical properties. The scaffolds prepared have an open, uniform and interconnected porous structure with a pore size of 200–400 mm. Compressive yield strength of ~ 5 MPa equivalents to that of cancellous bone and a compressive modulus of ~8 GPa similar to that of cortical bone were attained. Scanning electron microscope was used for the characterization of the pore

morphology, size, and distribution of the scaffolds were. X-ray diffraction and Fourier transform infrared spectroscopy were used to determine the crystal structure and chemical composition of scaffolds, respectively. Scaffolds with desired porosity, pore size, and geometry are prepared by using polymer sponges of desired structures.

(2) *Natural templates*[25, 29]

Natural replica templates include the cellular structures available in nature, which are used for fabrication of porous ceramics, mainly due to their special pore morphology and intricate microstructures. In recent years, a novel replica approach has been developed that uses wood structures as positive templates. Porous ceramics having highly oriented open pores ranging from 10 to 300 mm can be developed with this method at porosity levels between 25% and 95%.[25] The most crucial processing step in this route is the conversion of the wood-derived carbon preform into a ceramic phase.[29] The availability of templates exhibiting the desired microstructure is also essential in this process. The mechanical strength of wood-derived ceramics is highly anisotropic and often suffers from the presence of pores on the cell walls due to incomplete or inefficient conversion. The several steps required to convert the wood structures into the macro porous ceramic excessively increases the cost of the process. Fig. 2.2 shows a flow chart of the processing routes to transform cellular wood structures into porous ceramics

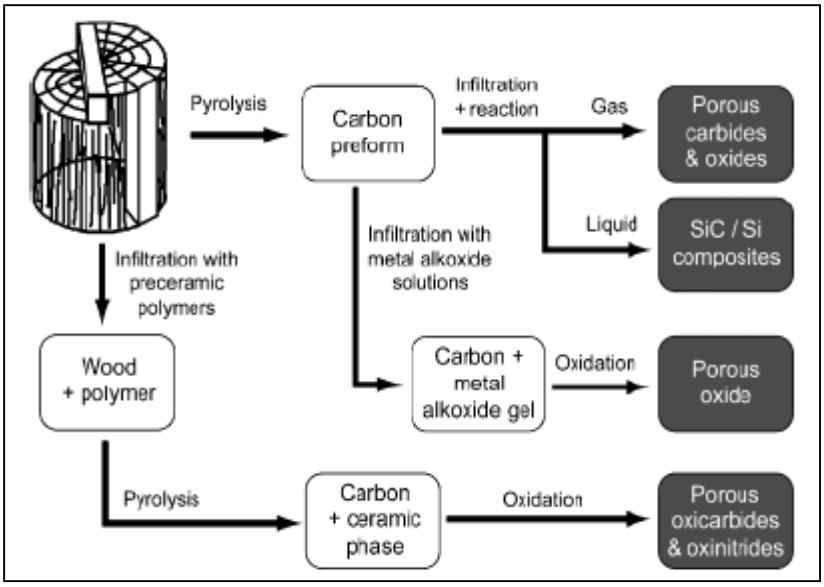

Fig. 2.2. Processing Routes to Transform Cellular Wood Structures into Porous Ceramics [30]

J. Cao et al.[31] found out a new method for preparation of microcellular ceramic materials through reproduction of wood morphologies by biotemplating. Biomorphic Al_2O_3-ceramics were produced by repeated infiltration of low viscous alumina sols into wood performs via the sol-gel route and then, sintered in air at 1550^{o}C. X-ray diffraction (XRD), scanning electron microscopy (SEM), density and porosimetry measurements were done in order to know about the microstructure and phase formation during processing. Depending on the initial wood template, the microstructure of the highly porous alumina ceramics is characterized by uniaxial pore morphology with pore diameter in the micrometer range.

2.3.2. ***Sacrificial Template Method***[25]

The sacrificial template technique includes preparation of a biphasic composite consisting of a continuous matrix of ceramic particles or ceramic precursors and a dispersed sacrificial phase that is initially homogeneously distributed throughout the matrix and is finally extracted to generate pores within the microstructure. Sacrificial templating methods provide an alternative for the fabrication of porous ceramics with porosities and average pore sizes ranging from 20%to 90% and 1–700 mm, respectively.[25] Predominantly open pores of various different morphologies can be produced. The most important step in this technique is the removal of the sacrificial phase by pyrolysis, evaporation, or sublimation. These processes might involve the release of an excessive amount of gases and have to be carried out at sufficiently slow rates in order to avoid cracking of the cellular structure. The slow removal of the sacrificial phase may substantially increase the processing time in the case of large components. The mechanical strength of cellular structures formed by this method is considerably higher than that achieved with the replica techniques. Fig. 2.3 exhibits the images of microstructures of macroporous ceramics produced with the sacrificial template method.

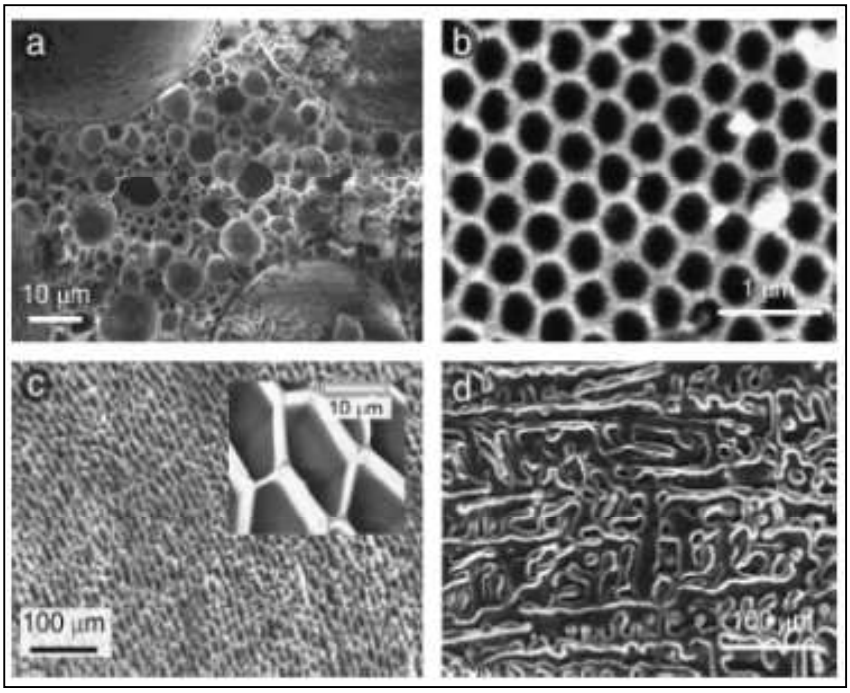

Fig. 2.3. Microstructures of macroporous ceramics produced with the sacrificial template method. (a) TiO_2 foam exhibiting hierarchical porous structure produced via emulsion templating (b) ordered macroporous SiO_2 obtained using polystyrene beads as templates (c) highly oriented SiO_2 honeycomb structure achieved via the unidirectional freeze-drying of silica gels (d) porous Al_2O_3 exhibiting dendrimer-like pores obtained using camphene as sacrificial template[25]

Dibyendu Chakravarty et al.[32] fabricated high strength porous alumina by spark plasma sintering at temperatures between 1000 and 1200 ◦C with nanocrystalline $Al(OH)_3$ as the starting powder without any seeds, dopants or inclusions. Decomposition of the $Al(OH)_3$ produced a series of transitional alumina phases depending on sintering temperature and pressure and finally the stable alumina phase was obtained. A network of continuous pores with unimodal pore size

distribution was found out by mercury porosimetry and BET surface area measurements, with the porosity ranging between 20% and 60% based on sintering conditions. Predominance of fine grains and extensive necking between them led to increased strength in the sintered samples. The bending strength of the sintered compacts rapidly increased with sintering temperature while retaining reasonable porosity suitable for practical applications. In situ phase formation of □-Al_2O_3 provided strength and porosity. Study of phase transformation, pore morphology and microstructure evolution was also done.

2.3.3. ***Direct Foaming Methods***[25-34]

In direct foaming methods, porous materials are produced by incorporating air into a suspension or liquid media, which is subsequently set in order to keep the structure of air bubble created.[25] The consolidated foams are sintered at high temperatures later to obtain high-strength porous ceramics. The total porosity of directly foamed ceramics is proportional to the amount of gas incorporated into the suspension or liquid medium during the foaming method. The pore size is determined by the stability of the wet foam before setting takes place.[33]

Direct foaming methods offer an easy, cheap, and fast way to prepare macroporous ceramics with open or closed porosities from 40% to 97%.[25] The pores produced with this approach result from the direct incorporation of air bubbles into a ceramic suspension, eliminating the need for extensive pyrolysis steps before sintering. Foams stabilized with surfactants lead to porous ceramics exhibiting average pore sizes from 35 mm to 1.2 mm.[25] The use of surface modified particles to stabilize the wet foam has decreased the lower limit of pore sizes achievable via direct foaming to an average value as low as 10 mm. Such small pore sizes

result from the long-term stability achieved through the irreversible adsorption of colloidal particles at the air–water interface. Cellular structures prepared by direct foaming usually exhibit mechanical strengths considerably higher than that of replica techniques due mainly to the absence of flaws in the cell struts. Compressive strengths as high as 16 MPa at a porosity level of 87 % to 90 % have been achieved with porous ceramics produced from particle-stabilized wet foams.[33]

Toshihiro Isobe et al.[34] prepared porous alumina ceramics having unidirectionally aligned cylindrical pores by extrusion method and compared them with porous ceramics having randomly distributed pores prepared by conventional method, and also investigated their gas permeability and mechanical properties. SEM micrographs of the porous alumina ceramics prepared, using nylon fibers as the pore former, through extrusion method showed excellent orientation of cylindrical pores. The bending strength and Weibull modulus of the extruded porous alumina ceramics with 39% porosity were 156 MPa and 17, respectively.These mechanical properties of extruded samples were estimated to be higher than those of the conventional porous alumina ceramics. The strength decreased from 156 to 106 MPa with increasing pore size from 8.5 to 38 μm. The gas permeability of the extrusion samples is also found to be higher than that of the conventional samples and increases along with increase in porosity and pore size.

2.4. *Need of Porous Bio-ceramics*

To satisfy the basic requirements in bone implant, we need:[35]

(1) A high porosity level for an organization of vascular canals that can ensure the blood supply

(2) Compatible mechanical properties with bone structure

(3) A high bioactivity for bone in-growth.

The substrate of the composite is strong, bio-inert porous matrix, which provides the mechanical strength needed for the structural bone.[36] The strength can also be altered by changing the dimension and density of the porosity, so that the composite is mechanically compatible to the human bone. A highly bioactive material, namely, hydroxyapatite (HA) is coated onto the inner surfaces of the pores in the substrate. In this way, the hard tissue can be in contact with a large surface that is bioactive. Bone ingrowth is well induced due to the high porosity level and the HA-coated pore surfaces. Fig. 2.4 shows the SEM micrographs of 90% porous hydroxyapatite.

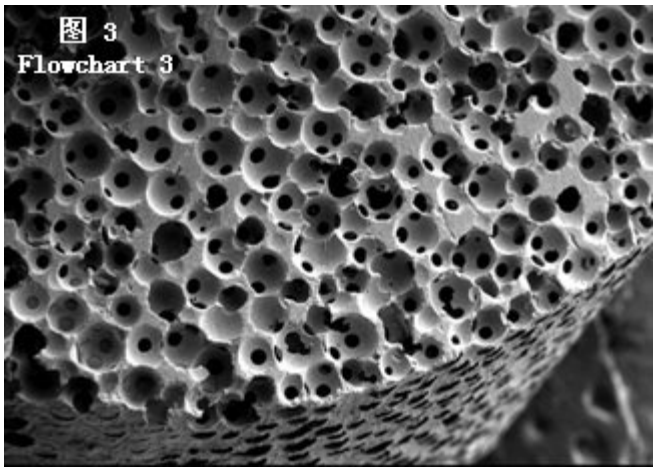

***Fig. 2.4. Picture of 90% Porous Alumina*[37]**

Emilie Chevalier et al.[36] reviewed solid and casting manufacturing processes able to create porous materials, mainly in the biomaterial field. The considered methods were based on pore forming agents that were removed either by heating or by dissolution. All techniques led to products presenting pores with amount, size, and shape close to those of the initial pore formers. Porosities up to 90% with pores ranging from 1 to 2000μm were reported.

2.5. *Porous Alumina as an Ideal Substrate for Bone Substitute*

In the development of bone substitutes, high porosity level is required for the following considerations:[38]

(1) Porous materials have large surface area, resulting in a high tendency to bioresorb, which induces high bioactivity.

(2) Interconnected pores permit tissue in-growth and thus anchor the prosthesis with the surrounding bone, preventing loosening of implants.

Interconnected porosity acts like an organization of vascular canals which can ensure the blood and nutrition supply for the bone. For serving this purpose, it is required that the dimension of the interconnected is at least 100 μm in diameter. According to these requirements, reticulated alumina has been chosen as the substrate material[38]. Alumina is not only bio-inert but also mechanically strong which makes it an ideal substrate for bone substitute. The high porosity is achieved via a sponge technique by which both pore size and density can be changed easily. The bioactivity is induced coating a HA film onto the inner pore surfaces of reticulated alumina. Other types of reticulated ceramics can also be used as substrate including ZrO_2 and MgO since they are chemically stable and mechanically strong. The most common applications

of porous ceramics, also called reticulated ceramics, are molten-metal and diesel engine exhaust filters. It can also be used as catalyst supports and industrial hot-gas filters, thermal insulators, and gas combustion burners.[38] Structurally, a reticulated material is porous matrix comprising interconnected voids surrounded by a web of ceramic, metal, or polymer. The open-cell nature of porous materials is a unique characteristic necessary for many applications. However, the surface-to-volume ratio of porous/reticulated materials is much larger than that of the dense materials, making them ideal for surface reaction applications.[38]

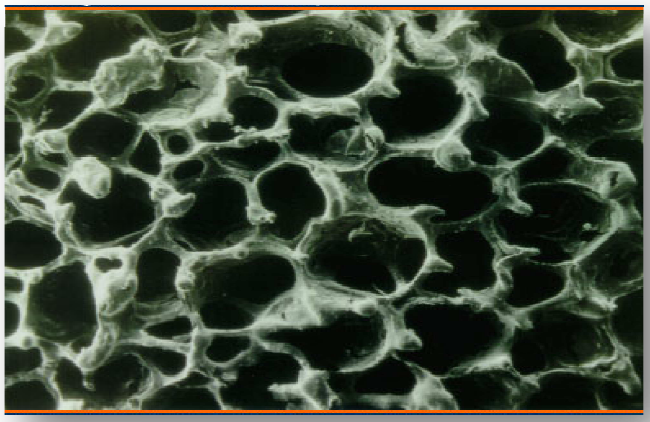

***Fig. 2.5. Porous Architecture Of Alumina (Bioceramic) Implant*[39]**

Weijiang Xue et al.[40] successfully fabricated alumina ceramic bodies with high porosity characterized by highly ordered and unidirectional oriented pores in the micrometer range with a 5-15 wt% solid loading range, by a self-organization process of alginate sol. The obtained porous alumina ceramics had a high total porosity over 70%, most (>88%) of which were open pores, as well as an excellent permeability ($K>2.16 \times 10^{-11}$ m^2) and high compressive strength (>15 MPa).

2.6. ***Objective***

The preceding discussion on the processing of porous alumina reveal that processing route plays an important role for maintaining a porous structure with interconnectivity. On the basis of literature review, the following studies are being planned.

- → Processing alumina based porous ceramics through naphthalene as the pore former.
- → To study the porosity and strength as function of pore former amount, sintering temperature and time.
- → To characterize porous ceramics with respect to strength, porosity and microstructure.
- → To study the porosity and pore size distribution through mercury porosimetry.

\

CHAPTER-3: EXPERIMENTAL DETAILS

3.1. *Preparation of green pellets of alumina with naphthalene*

3.1.1. *Raw materials and batch calculation*

The specifications of raw materials are given below:

1) Reactive Alumina from NALCO, chemical formula : Al_2O_3
2) Naphthalene from LOBA Chemie, chemical formula : $C_{10}H_8$
3) PVA from LOBA Chemie, chemical formula : $(C_2H_4O)n$

Batch calculation

Diameter of the die to be used while pressing – 12.5 mm diameter

Thickness of the pellets to be made = 6 mm

Volume of each pellets = $\pi D^2 h/4$

$= 3.14(1.25)^2(0.6)/4\ cm^3$

$= 0.7363$ cc

(A) Sample preparation of 100% alumina

Loose Fill Density (LFD) of the alumina sample = 3 gm/cc

Loose Fill Density (LFD) of the naphthalene sample = 1.9 gm/cc

Loose Fill Density (LFD) was used to calculate the mixed composition because in the fine powder, theoretical density cannot be achieved.

Mass of 1 pellet = Volume of each pellet x Theoretical density of the sample

= 0.7363 cc x 3 gm/cc

= 2.21 gm

50 pellets are to be made.

Therefore, total calculated mass of all the 50 pellets = 50 x 2.21gm

= 110.45 gm

The green density on compaction will be only 50%, i.e. it will contain 50% voids or pores. Hence, green density will be 50% of the theoretical density.

Since, Green density = (Theoretical density)/2

So, actual mass of 50 pellets to be made = Calculated mass/2

= 110.45/2 gm

= 55.22 gm

(B) Sample preparation of 80% alumina + 20 % naphthalene

Theoretical density of the sample = (Density of alumina x Weight fraction of alumina) + (Density of naphthalene x Weight fraction of naphthalene)

= (3 gm/cc x 0.8) + (1.9 gm/cc x 0.2)

= 2.78 gm/cc

Mass of 1 pellet = Volume of each pellet x Theoretical density of the sample

= 0.7363 cc x 2.78 gm/cc

= 2.0469 gm

50 pellets are to be made.

Therefore, total calculated mass of all the 50 pellets = 50 x 2.0469 gm

= 102.34 gm

Since, Experimental density = (Theoretical density)/2

So, actual mass of 50 pellets to be made = Calculated mass/2

= 102.34/2 gm

= 51.17 gm

For 80% alumina, we need 80 gm alumina in 100 gm batch.

Hence, in 51.17 gm batch, we need (80 x 51.17)/100 gm alumina = 40.94 gm alumina.

For 20% naphthalene, we need 20 gm naphthalene in 100 gm batch.

Hence, in 51.17 gm batch, we need (20 x 51.17)/100 gm naphthalene = 10.234 gm naphthalene

Similarly, calculations were done for the preparation of the other compositions.

Table 3.1. Batch Calculation done for the Sample Preparation

Sample specifications	*Weight of alumina (gm)*	*Weight of naphthalene (gm)*
100% alumina	55.22	–
80% alumina and 20 % naphthalene	40.94	10.23
70% alumina and 30 % naphthalene	34.40	14.74
60% alumina and 40 % naphthalene	28.27	18.85
50% alumina and 50 % naphthalene	22.55	22.55

3.1.2. 8*% PVA binder solution preparation*

Polyvinyl alcohol was obtained from LOBA Chemie [chemical formula: $(C_2H_4O)_n$]. The binder solution was prepared following the steps mentioned in the Fig. 3.1.

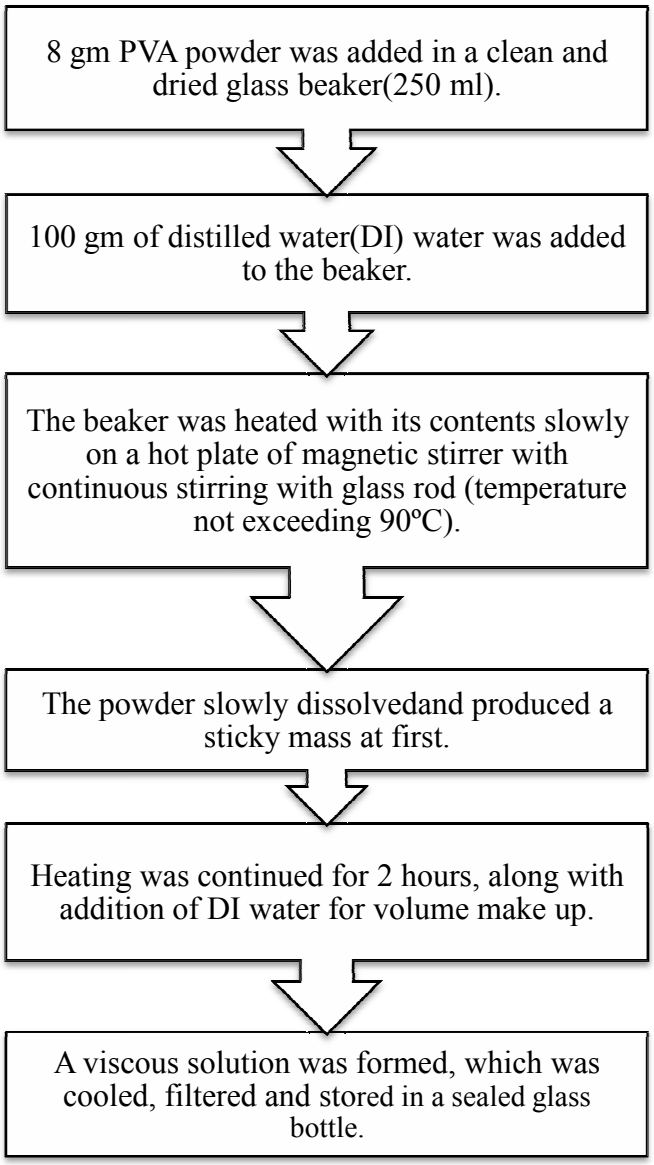

Fig. 3.1. Flow chart for 8% PVA binder solution preparation

3.1.3. ***Mixing and drying of batch***

Green alumina and alumina-naphthalene pellets were prepared using 75μm fine reactive alumina powder and naphthalene of size (-300 + 200) μm. At first, calculated amount of reactive alumina powder was weighed and dry mixed thoroughly in an agate mortar pestle with the required amount of naphthalene (to form 5 types of samples). This was followed by addition of desired volume of PVA solution so that final PVA content of the batch was 6%. The PVA solution was thoroughly blended with alumina by mixing it in agate mortar for 30 minutes whereby the blended mass was of paste consistency. The paste was air dried for one day followed by drying in oven (100^{o}C) for another 24 hours. After complete drying, the hardened mass was finely ground in the agate mortar. The dry ground powder was then weighed to the required amount for making the pellets.

3.1.4. ***Green compaction***

Pellets were made by dry pressing in a hydraulic press (Carver Press USA) at a load of 3.5 MPa, with a 25% pump speed and dwell time of 90 seconds. A high carbon, high chrome steel die (12.5 mm diameter) was used. The pellet thickness was 6 mm. Acetone was used for cleaning the die to prevent contamination and sticking and 5% stearic acid solution was used for lubrication.

3.1.5. ***Drying of green pellets***

Green pellets formed by dry pressing were dried for one day in oven (100^{o}C).

3.2. *Sintering of green pellets*

The pressed pellets were sintered in an electrical resistance heating furnace (Bysakh & Co.) with $MoSi_2$ heating element at 1500ºC, 1550ºC and 1600ºC. At each sintering temperature, the holding times for different batches were 2, 3 and 4 hours. An intermediate soaking period of 1 hour at 600ºC was provided for binder removal. The samples were heated at 3ºC/min till 600ºC followed by heating at 3ºC/min till the final sintering temperature. Following the holding at the final temperature, the furnace was switched off for cooling and the samples were taken after the furnace temperature reached below 100ºC.

3.3. *Characterization of raw materials and sintered pellets*

3.3.1. *DSC/TG of naphthalene*

The DSC/ TG experiments were conducted in a Netzsch 449C Thermal Analyser. The samples were heated in flowing Ar gas atmosphere at a heating rate of 5ºC/min. The weight loss measurements were also done in the same instrument.

3.3.2. *Dilatometer of Alumina and Alumina - Naphthalene Samples*

A dilatometer is a scientific instrument that measures volume changes caused due to any physical or chemical process. Dilatometry is also used to supervise the progress of chemical reactions. Measurement of thermal expansion is the common application of a dilatometer. Connecting rod (push rod) dilatometer was used to find out the sintering and shrinkage behavior and the range of temperatures. The samples were heated at a heating rate of 5ºC/min till 1500^{o}C.

3.3.3. ***Apparent Porosity, Bulk Density Measurements***

The densities of green pellets were determined from the weight and volume. 3 pellets from each type of samples were taken and density was measured. Average of the 3 density measurements were taken into consideration. The following formula was used to measure the density of green pellets: Density = (Mass of pellet)/(Volume of cylindrical pellet)

The apparent porosity, bulk density of sintered pellets was measured. First the dry weight of pellets was measured. Then they were soaked in kerosene kept inside a beaker and were evacuated in a vacuum evacuator till all the air bubbles vanished. After that they were kept inside vacuum for few hours. After removing from vacuum evacuator, the suspended weight and soaked weight of the samples were calculated.

To obtain bulk density (B.D.), the following formula was used:

B.D. = (dry weight)/(soaked weight - suspended weight)

---------- (3.1)

To obtain apparent porosity (A.P.) in %, the formula used is:

A.P. = (soaked weight - dry weight)*100/(soaked weight - suspended weight)

---------- (3.2)

3.3.4. ***Compressive Strength (CCS) Measurements***

The compressive Strength of the pellets was measured by breaking the samples in a Tinius Olsen Materials Testing Machine (HK10S model). It has a maximum load capacity of 10 KN. The compressive strength, CCS was obtained using the formula:

$$CCS = P/A \qquad \text{---------- (3.3)}$$

where, P = Maximum Load

A= Area of the cylindrical pellet

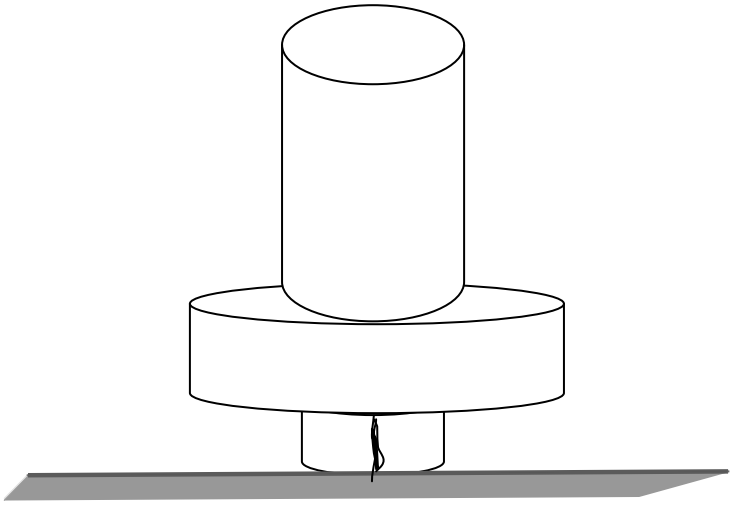

Fig. 3.2. Compressive Strength Test Showing Loading and Fracture Mode

3.3.5. ***Bi-axial Tensile Strength Measurements***

The bi-axial tensile strength of the pellets was measured by breaking the samples in a Tinius Olsen Materials Testing Machine (HK10S model). It has a maximum load capacity of 10 KN. The bi-axial tensile strength, S was obtained using the formula:

$$S = (2*P)/ (\Pi*D*t) \qquad \text{---------- (3.4)}$$

where, P = Maximum Load

D = Diameter of the pellet

t = Thickness of the pellet

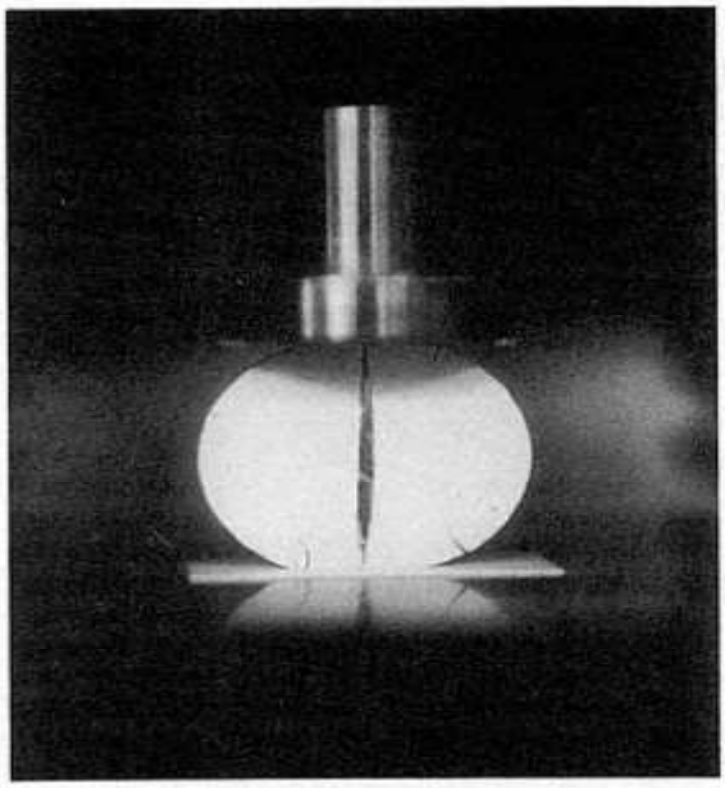

Fig. 3.3. Diametral Compression Test Showing Loading and Fracture Mode[42]

3.3.6. ***Pore Size Distribution by Porosimeter Test***

Mercury porosimetry is an extremely useful characterization technique for porous ceramics. Pores of about 500μm to 3.5 nm can be investigated. Mercury porosimetry provides a wide range of information, e.g. the pore size distribution, the total volume or porosity, the skeletal and apparent density, and the specific surface area of a sample. Mercury porosimetry does not actually measure the internal pore size; rather it determines the largest connection from the sample surface towards that pore. Thus, mercury porosimetry results will always show smaller pore sizes compared with SEM or optical micrographs. The pellets fired at 1500□C for 2

hours were chosen for porosimeter test. Intrusion pressure of range 0.863 PSIA to 31.868 KPSIA and extrusion pressure range of 31.594 KPSIA to 22.378 PSIA was applied. Penetrometer constant is 1604 mv/cc.

3.3.7. *Optical Microscope Imaging*

The selected sintered samples were viewed in optical microscope. The images were taken using Olympus optical microscope fitted with a CCTV camera using Image analysis software. Magnifications of 10X, 20X and 50X was used while procuring the images. The pellets were placed on a slide and then viewed through the monitor screen. The pellets fired at 1500□C for 2 hours were chosen for optical imaging.

3.3.8. *Scanning Electron Microscopy (SEM)*

Scanning Electron Microscope provides topographical and elemental information at magnifications of 10X to 100,000X with unlimited depth of field. A finely focused electron beam scanned across the sample surface generates secondary electrons, backscattered electrons, and characteristic X-rays. These signals are gathered by detectors to form images of the sample displayed on a cathode ray tube screen. Data Output is generated on the CRT monitor. Images and spectra can be printed here, or recorded on CD ROM. Pellets fired at 1600□C for 3 hours were chosen for SEM.

CHAPTER – 4
RESULTS AND DISCUSSIONS

4.1. ***Thermal Analysis of Naphthalene:***

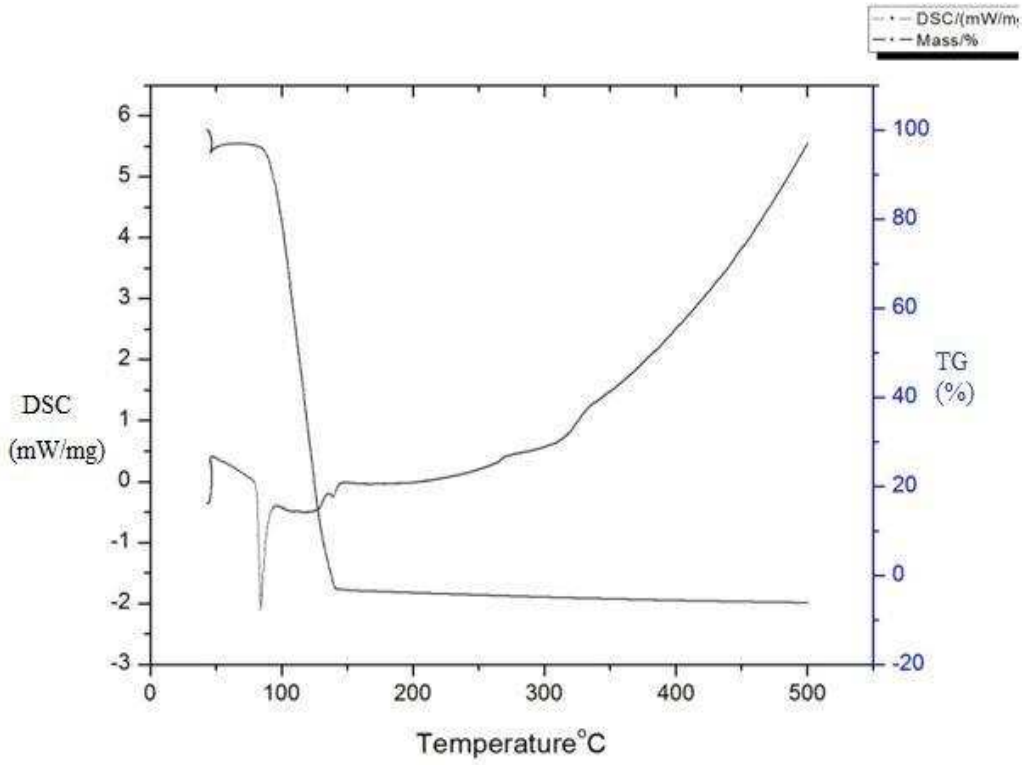

Fig. 4.1. DSC-TG Plot for Naphthalene Heated in Air at 5ºC/min Heating Rate

DSC/TG plot of naphthalene at 5ºC/min heating rate shows a sharp and distinct endothermic peak at around 86ºC, a broad endothermic peak at 125ºC and another small endothermic peak at 150^{o}C. The sharp endothermic peak at 86^{o}C is due to fusion of naphthalene. This peak can be assigned to decomposition and volatilization of naphthalene. No further major weight loss was observed beyond this temperature. TG curve shows that by 150^{o}C, the weight loss of naphthalene is completed.

4.2. ***Sintering Behavior of Alumina:***

The shrinkage plots for pure alumina and alumina with different fractions of naphthalene are shown in Fig. 4.2 – 4.6. All the plots show a maximum expansion followed by shrinkage. The onset of shrinkage marks the start of densification process. Accordingly, pure alumina starts densifying at around 1100^{o}C (Fig. 4.2), while with naphthalene, the onset of densification temperature shifts to higher temperature (>1200^{o}C).

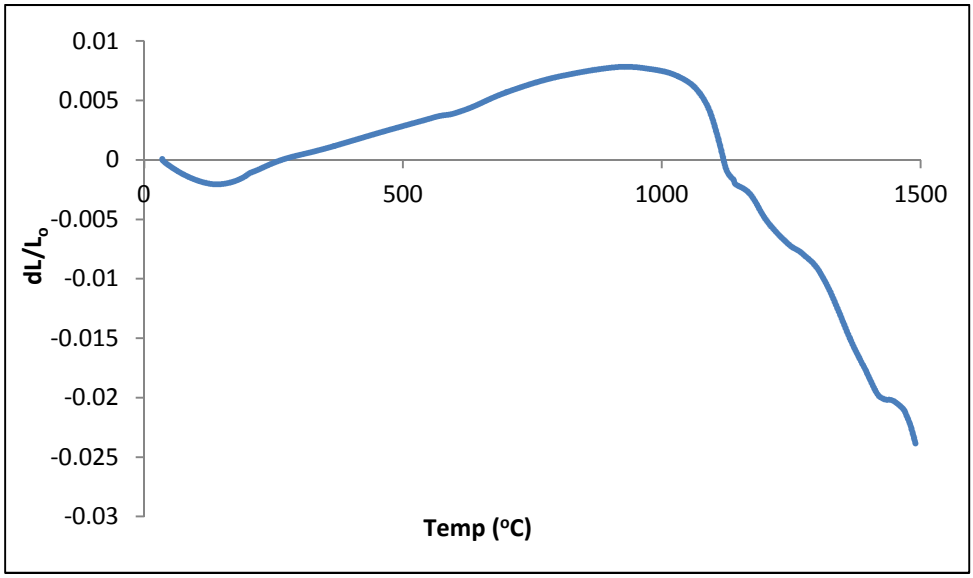

Fig 4.2. Dilatometry Curve of Pure Alumina

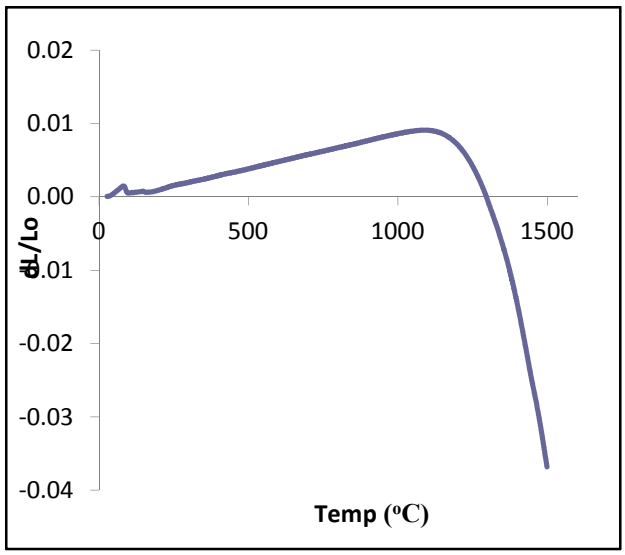

Fig 4.3. Dilatometry Curve of 80% Alumina and 20% Naphthalene

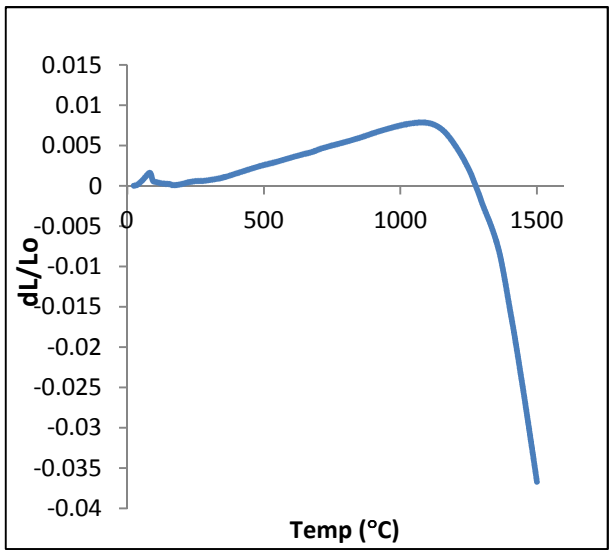

Fig 4.4. Dilatometry Curve of 70% Alumina and 30% Naphthalene

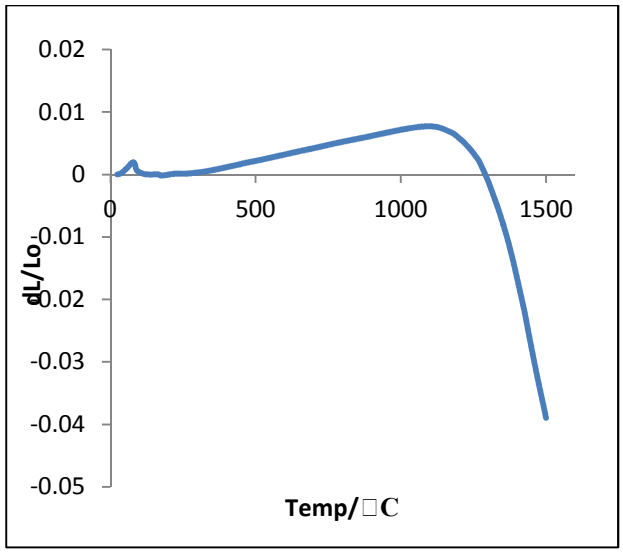

Fig 4.5. Dilatometry Curve of 60% Alumina and 40% Naphthalene

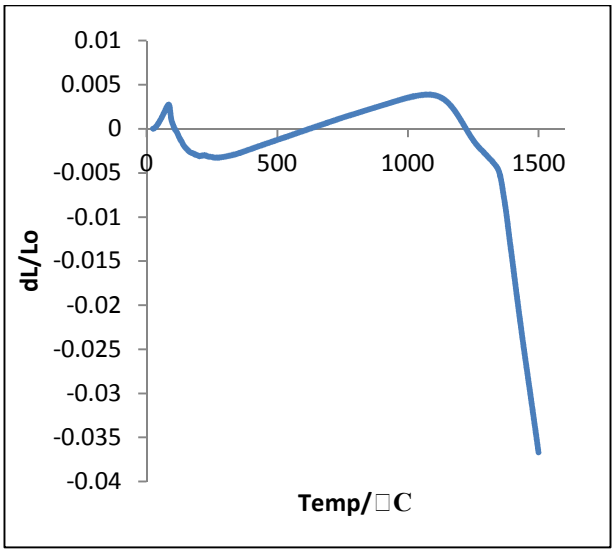

Fig 4.6. Dilatometry Curve of 50% Alumina and 50% Naphthalene

Thus, the addition of naphthalene create pores in the green compact of alumina which requires higher sintering temperature for its removal and shrinkage. Thus, at a particular temperature, alumina (containing naphthalene as pore former) will be more porous than pure alumina.

4.3. *Apparent Porosity and Bulk Density of Sintered Pellets:*

4.3.1. *Apparent Porosity:*

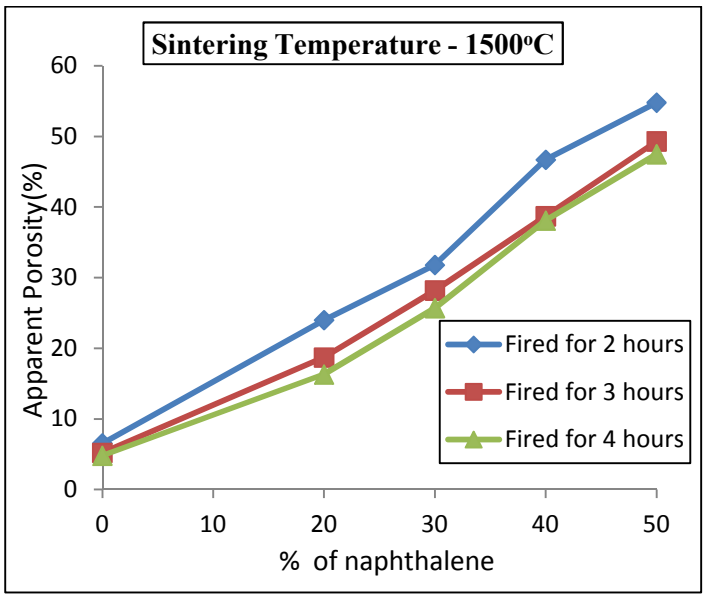

Fig. 4.7. Variation in Apparent Porosity of Fired Samples (Fired at 1500°C) due to Change in Sintering Time and percentage of Naphthalene

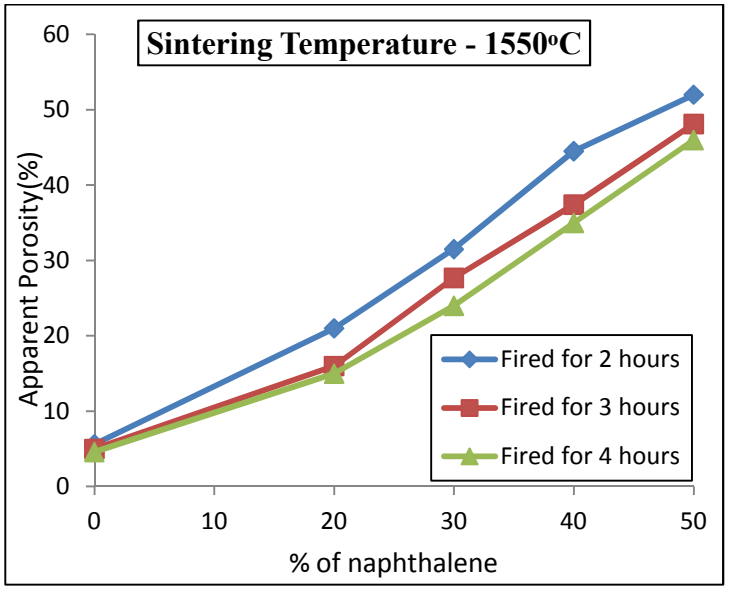

Fig. 4.8. Variation in Apparent Porosity of Fired Samples (Fired at 1550°C) due to Change in Sintering Time and percentage of Naphthalene

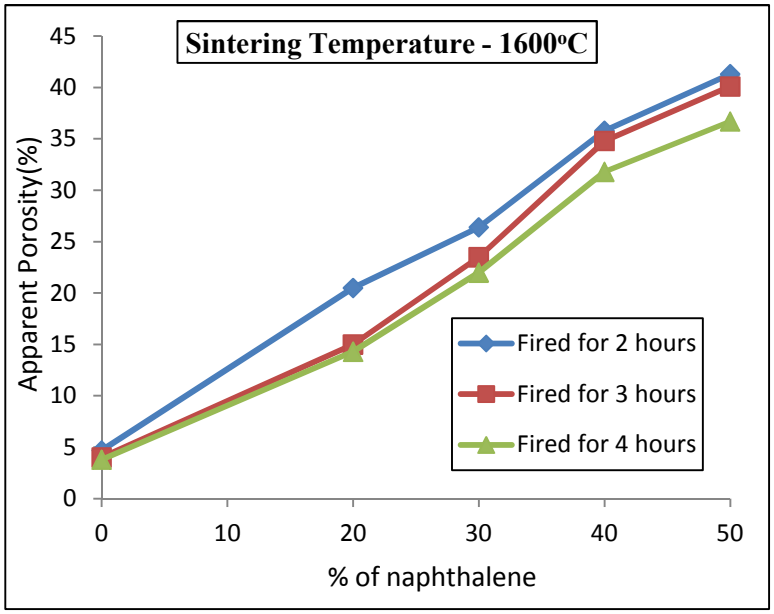

Fig. 4.9. Variation in Apparent Porosity of Fired Samples (Fired at 1600°C) due to Change in Sintering Time and percentage of Naphthalene

Fig. 4.7 – 4.9 shows the variation of apparent porosity in the sintered alumina and alumina – naphthalene as a function of naphthalene content for different sintering temperature and holding time combinations. All the plots show similar i.e. increasing porosity trend with naphthalene content. However, the absolute value of porosity decreases with an increase in sintering temperature and time. This implies that at higher sintering temperature and/or longer holding time, the pore mobility increases. This causes reduction in porosity. Table 4.1 shows the variation in apparent porosity for all the different batches of samples.

Table 4.1. Summary of Apparent Porosity of Sintered Pellets of all compositions of Alumina – Naphthalene composition

Volume% Naphthalene	*Sintering Time*	*Volume% Apparent Porosity at different Sintering Temperature*		
		1500^{o}C	*1550^{o}C*	*1600^{o}C*
0	2	6.5	5.6	4.7
	3	5.2	5	4
	4	4.8	4.6	3.8
20	2	24	21	20.5
	3	18.7	16	15.
	4	16.3	15	14.3
30	2	31.8	31.5	26.4
	3	28.2	27.7	23.5
	4	25.7	24	22
40	2	46.7	44.5	36.8
	3	38.7	37.4	35.8
	4	38.1	35	31.8
50	2	54.8	52	41.3
	3	49.3	48.1	40.1
	4	47.5	46	36.7

4.3.2. ***Bulk Density:***

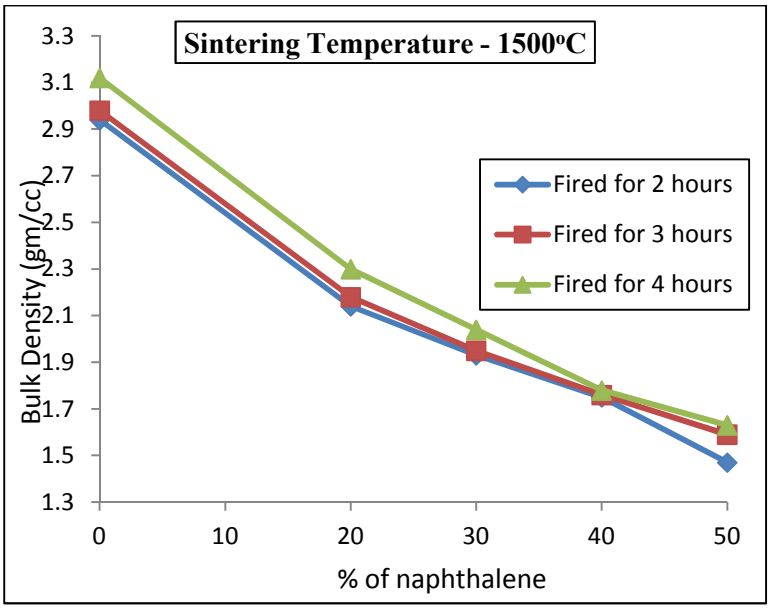

Fig. 4.10. Variation in Bulk Density of Fired Samples (Fired at 1500°C) due to Change in Sintering Time and percentage of Naphthalene

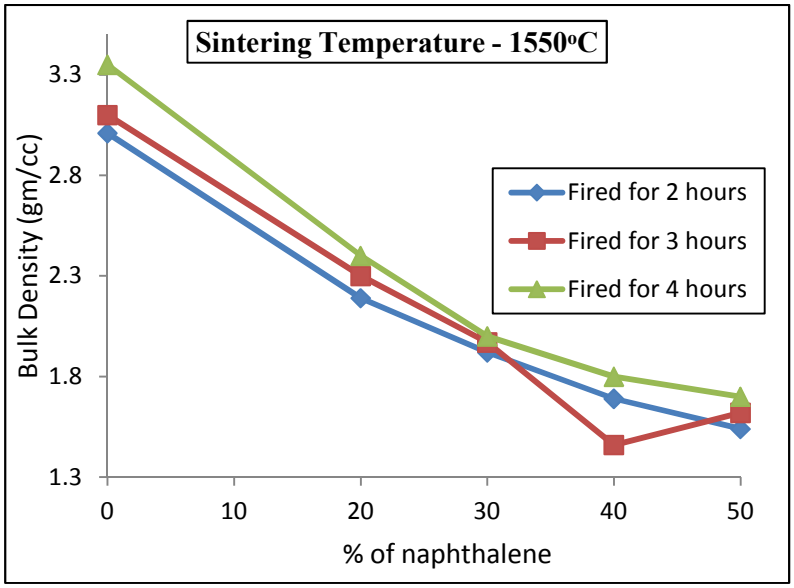

Fig. 4.11. Variation in Bulk Density of Fired Samples (Fired at 1550°C) due to Change in Sintering Time and percentage of Naphthalene

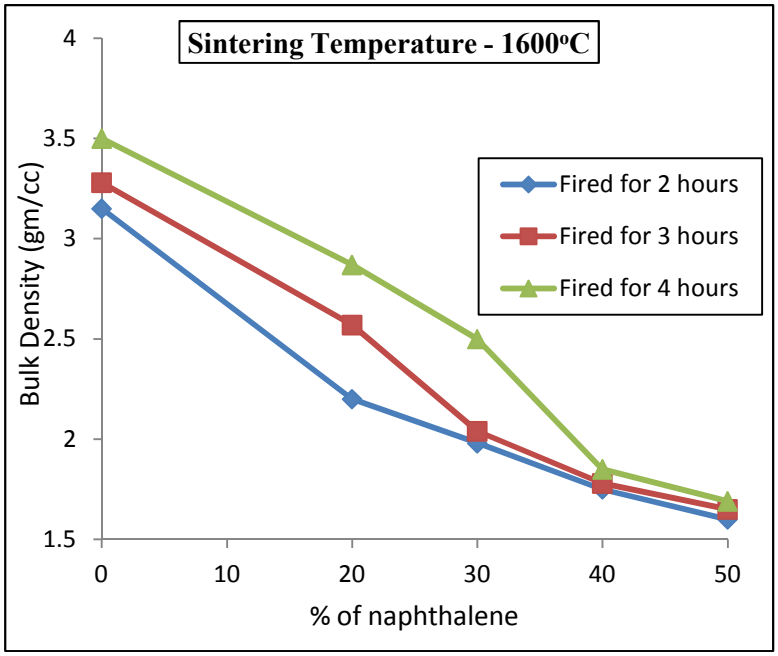

Fig. 4.12. Variation in Bulk Density of Fired Samples (Fired at 1600°C) due to Change in Sintering Time and percentage of Naphthalene

Fig. 4.10 – 4.12 shows the variation of bulk density in the sintered alumina and alumina – naphthalene as a function of naphthalene content for different sintering temperature and holding time combinations. All the plots show similar i.e. decreasing bulk density trend with naphthalene content. However, the absolute value of bulk density increases with an increase in sintering temperature and time. This implies that at higher sintering temperature and/or longer holding time, the pore mobility increases. This causes reduction in porosity and increase in bulk density. Table 4.2 shows the variation in bulk density for all the different batches of samples.

Table 4.2. Summary of Bulk Density of Sintered Pellets of all compositions of Alumina – Naphthalene composition

Volume% Naphthalene	*Sintering Time*	*Bulk Density (gm/cc) at different Sintering Temperature*		
		1500^{o}C	*1550^{o}C*	*1600^{o}C*
0	2	2.94	3.01	3.15
	3	2.98	3.1	3.28
	4	3.12	3.35	3.5
20	2	2.12	2.19	2.25
	3	2.2	2.3	2.57
	4	2.3	2.4	2.87
30	2	1.93	1.92	1.98
	3	1.95	1.97	2.04
	4	2.04	2	2.5
40	2	1.75	1.69	1.75
	3	1.76	1.46	1.78
	4	1.78	1.8	1.85
50	2	1.47	1.54	1.6
	3	1.59	1.62	1.65
	4	1.63	1.7	1.75

4.4. *Compressive and Bi-axial Flexural Strength*

4.4.1. *Variation in Compressive Strength (CCS) with Porosity*

Fig. 4.13 – 4.15 shows that CCS is higher for pure alumina in comparison to alumina – naphthalene samples due to higher porosity in the latter samples. Higher porosity implies less load bearing capacity and weak samples. Therefore, the strength decreases at higher naphthalene content.

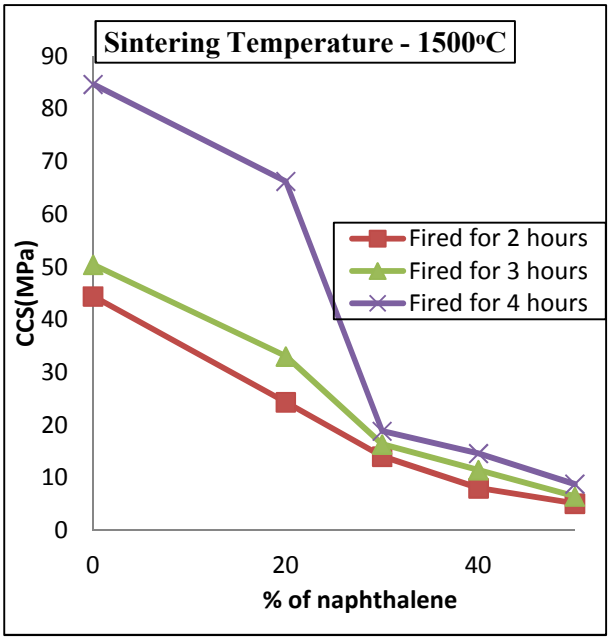

Fig. 4.13. Variation in CCS of Fired Samples (Fired at 1500°C) due to Change in Sintering Time and percentage of Naphthalene

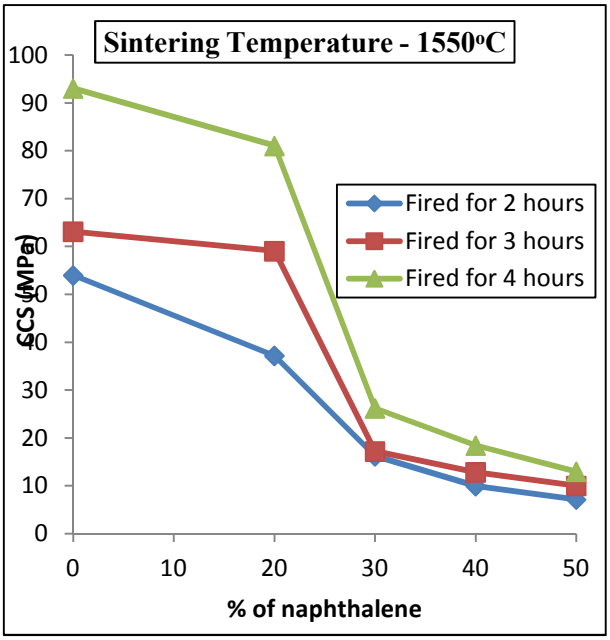

Fig. 4.14. Variation in CCS of Fired Samples (Fired at 1550°C) due to Change in Sintering Time and percentage of Naphthalene

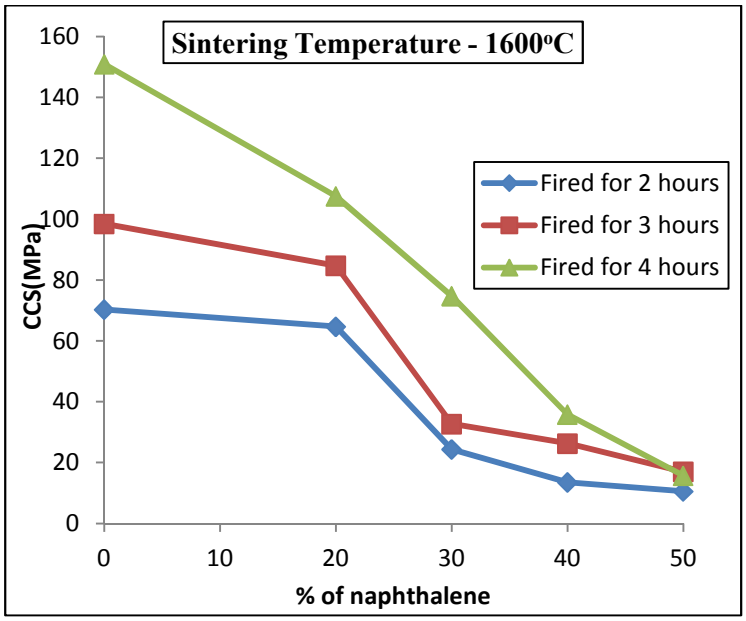

Fig. 4.15. Variation in CCS of Fired Samples (Fired at 1600°C) due to Change in Sintering Time and percentage of Naphthalene

As the sintering temperature or holding time increases, the strength increases because at higher sintering temperature and/or longer sintering time, the porosity of the samples decreases i.e. the samples densify. This increases the load bearing capacity or in other words, strength increases. Table 4.3 shows the variation of CCS for all combinations of samples and their sintering schedules.

Table 4.3. Summary of CCS of Sintered Pellets of all compositions of Alumina – Naphthalene composition

Volume% Naphthalene	*Sintering Time*	*CCS (MPa) at different Sintering Temperature*		
		1500^{o}C	*1550^{o}C*	*1600^{o}C*
0	2	44.4	54	70.3
	3	50.4	63	98.5
	4	84.7	93	151
20	2	24.3	37.2	64.7
	3	33	59	84.7
	4	66.2	81	107.6
30	2	14	16.2	24.4
	3	16.4	17.2	32.7
	4	18.8	26.2	74.7
40	2	8	10	13.5
	3	11.5	12.8	26.3
	4	14.6	18.4	35.8
50	2	5	7	10.6
	3	6.5	10	17
	4	8.8	13	15.7

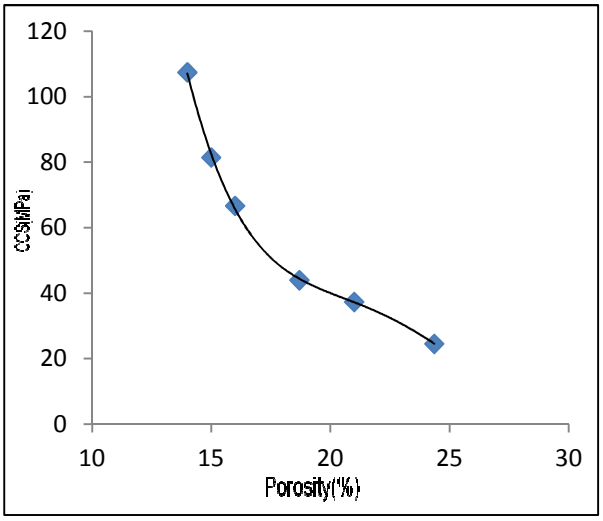

Fig. 4.16. CCS vs porosity for 80% alumina and 20% naphthalene

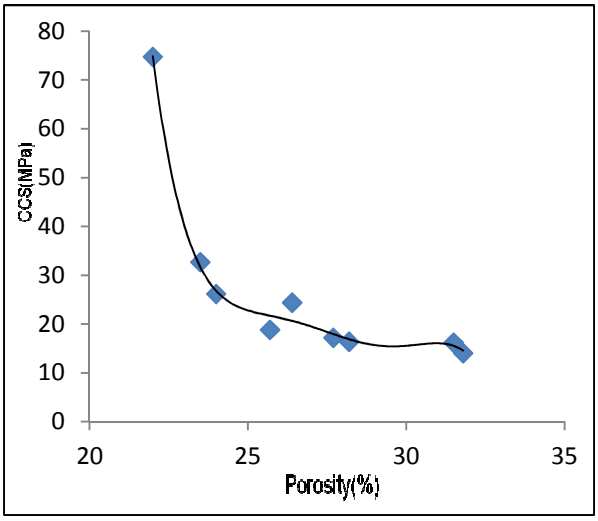

Fig. 4.17. CCS vs porosity for 70% alumina and 30% naphthalene

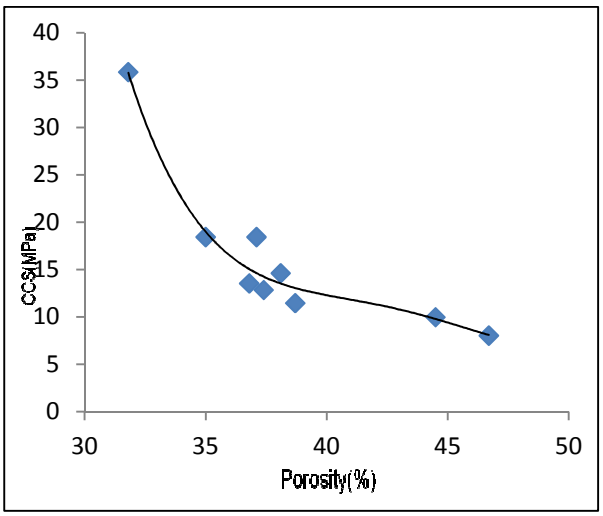

Fig. 4.18. CCS vs porosity for 60% alumina and 40% naphthalene

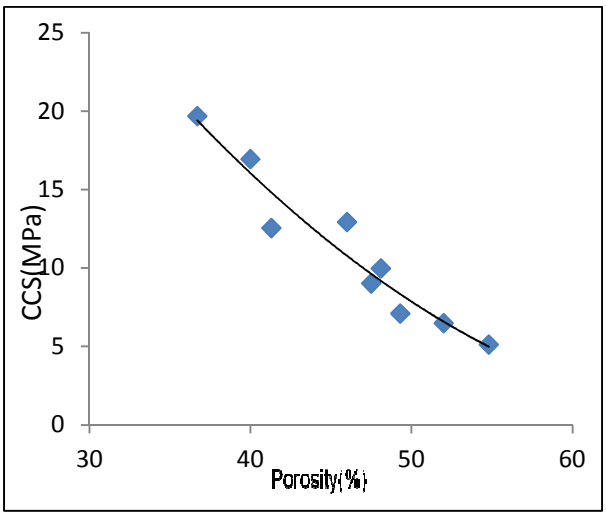

Fig. 4.19. CCS vs porosity for 50% alumina and 50% naphthalene

Fig. 4.16 – 4.19 show the variation of strength with porosity. The plots show that the strength decreases exponentially with temperature which proves that the strength follows the relation $\sigma \alpha \exp(-bp)$ where b is a constant and p is the volume percent porosity.

When lnσ was plotted against porosity, the plots show a linear fit with a negative slope. The value of b was calculated from the slope of the curve and it varied between 0.07 – 0.135 for varying amount of naphthalene.

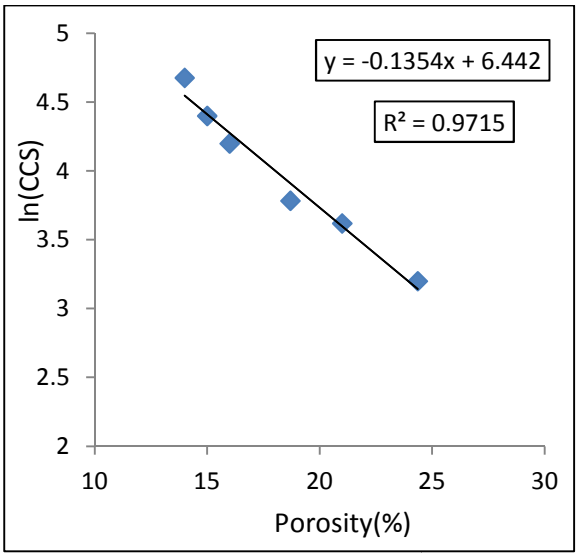

Fig. 4.20. ln(CCS) vs porosity for 80% alumina and 20% naphthalene

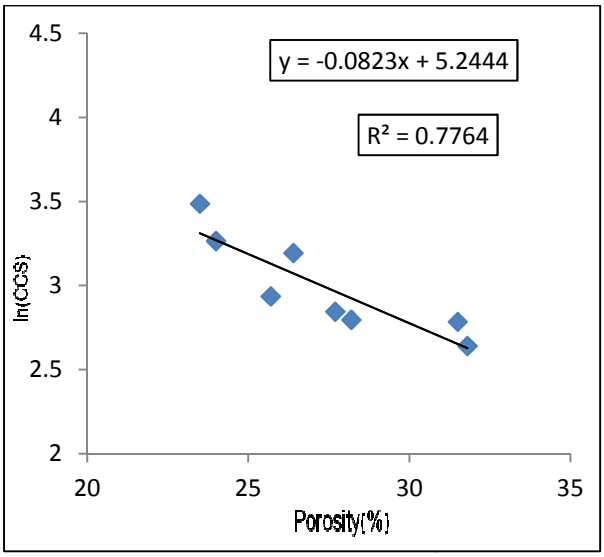

Fig. 4.21. ln(CCS) vs porosity for 70% alumina and 30% naphthalene

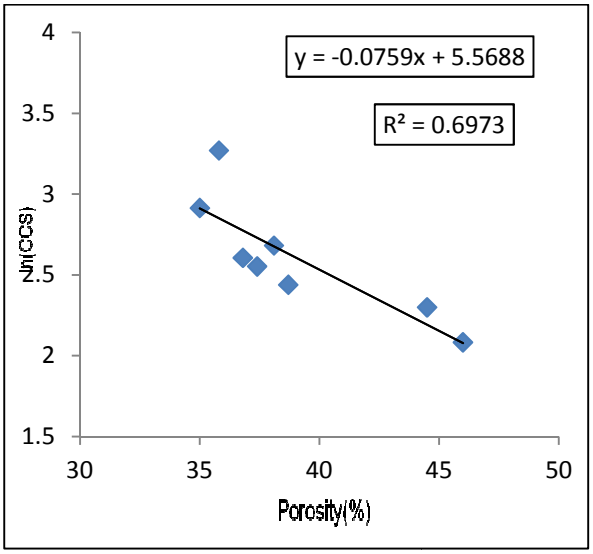

Fig. 4.22. ln(CCS) vs porosity for 60% alumina and 40% naphthalene

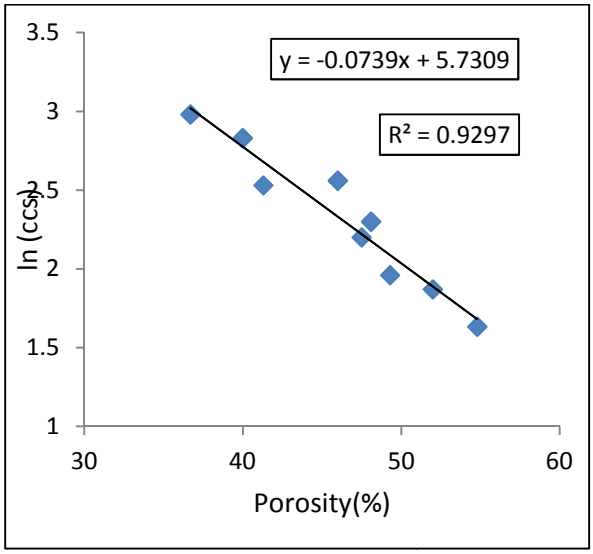

Fig. 4.23. ln(CCS) vs porosity for 50% alumina and 50% naphthalene

4.4.2. ***Variation in Bi-axial Flexural Strength with Porosity***

Fig. 4.24 – 4.26 shows that the bi-axial flexural strength is higher for pure alumina in comparison to alumina – naphthalene samples due to higher porosity in the latter samples. Higher porosity implies less load bearing capacity and weak samples. Therefore, the flexural strength decreases at higher naphthalene content. Further, the samples tested in bi-axial flexural test mode are subjected to bi-axial tensile force which acts on both surface perpendicular to the direction of load application. Hence, the bi-axial flexural strength is lower than compressive strength.

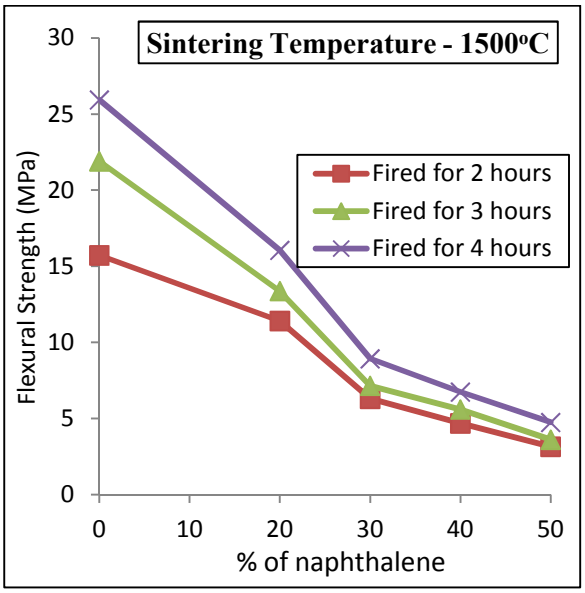

Fig. 4.24. Variation in Flexural Strength of Fired Samples (Fired at 1500°C) due to Change in Sintering Time percentage of Naphthalene

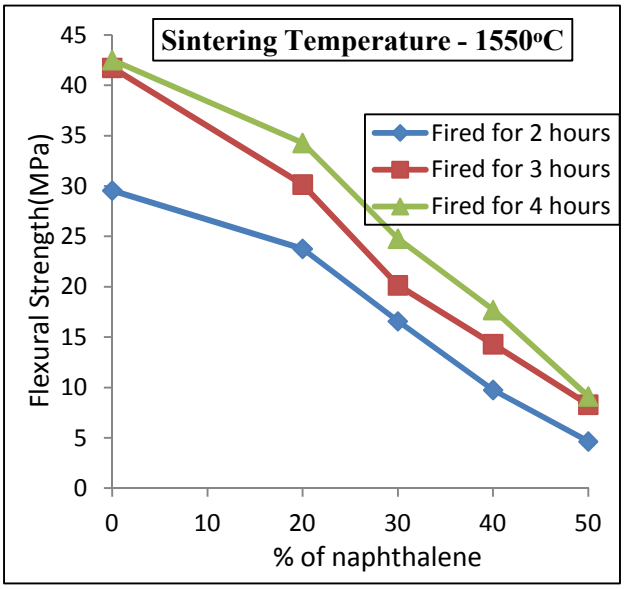

Fig. 4.25. Variation in Flexural Strength of Fired Samples (Fired at 1550°C) due to Change in Sintering Time and percentage of Naphthalene

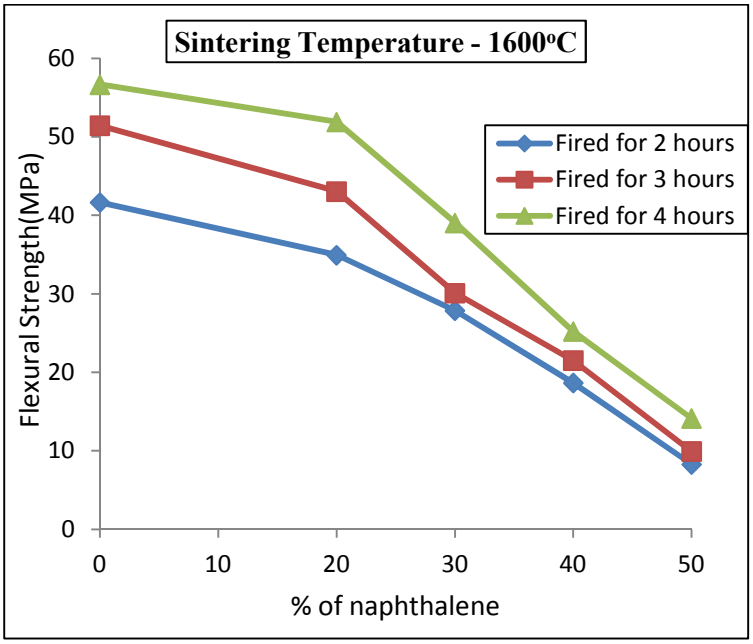

Fig. 4.26. Variation in Flexural Strength of Fired Samples (Fired at 1600°C) due to Change in Sintering Time and percentage of Naphthalene

As the sintering temperature or holding time increases, the flexural strength increases because at higher sintering temperature and/or longer sintering time, the porosity of the samples decreases. This increases the load bearing capacity or in other words, strength increases. Table 4.4 shows the variation of flexural strength for all combinations of samples and their sintering schedules.

Table 4.4. Summary of Bi-axial Flexural Strength of Sintered Pellets of all compositions of Alumina – Naphthalene composition

Volume % naphthalene	*Sintering time(hours)*	*Flexural strength (MPa) at different Sintering Temperature*		
		1500^oC	*1550^oC*	*1600^oC*
0	2	15.7	29.6	41.7
	3	22	41.8	51.4
	4	26	42.5	56.7
20	2	11.4	23.8	35
	3	13.4	30.2	43
	4	16	34.3	51.8
30	2	6.3	16.6	27.8
	3	7.2	20.2	30.2
	4	9	24.8	39
40	2	4.7	9.8	18.7
	3	5.6	14.4	21.5
	4	6.7	17.7	25.2
50	2	3.2	4.7	8.3
	3	3.6	8.3	10
	4	4.7	9.2	14

4.5. ***Porosimetry and Pore Size Distribution***

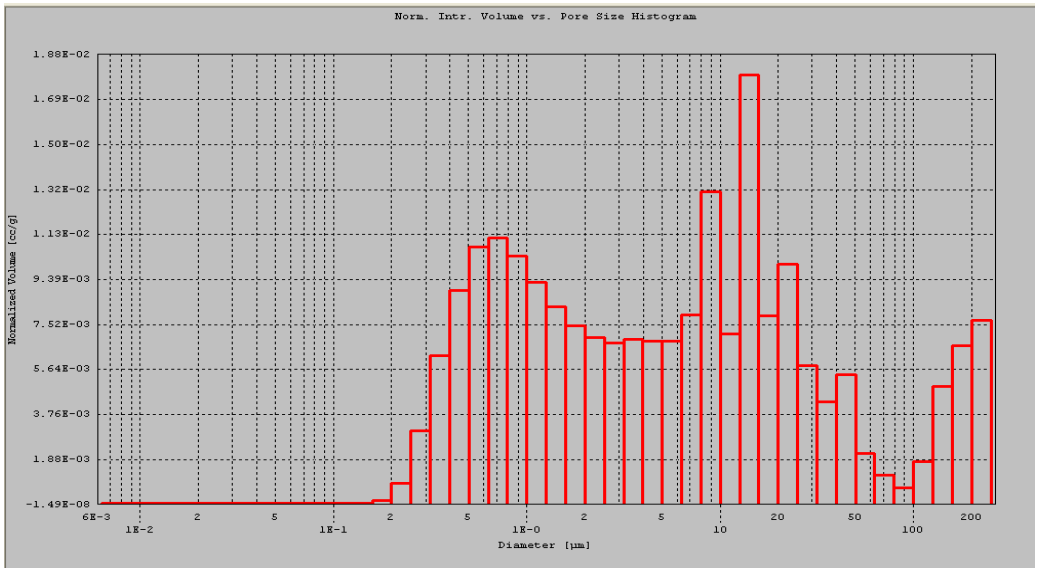

Fig. 4.27. Cumulative distribution analysis of 80% Alumina and 20% Naphthalene sample fired At 1500□C for 2 hrs

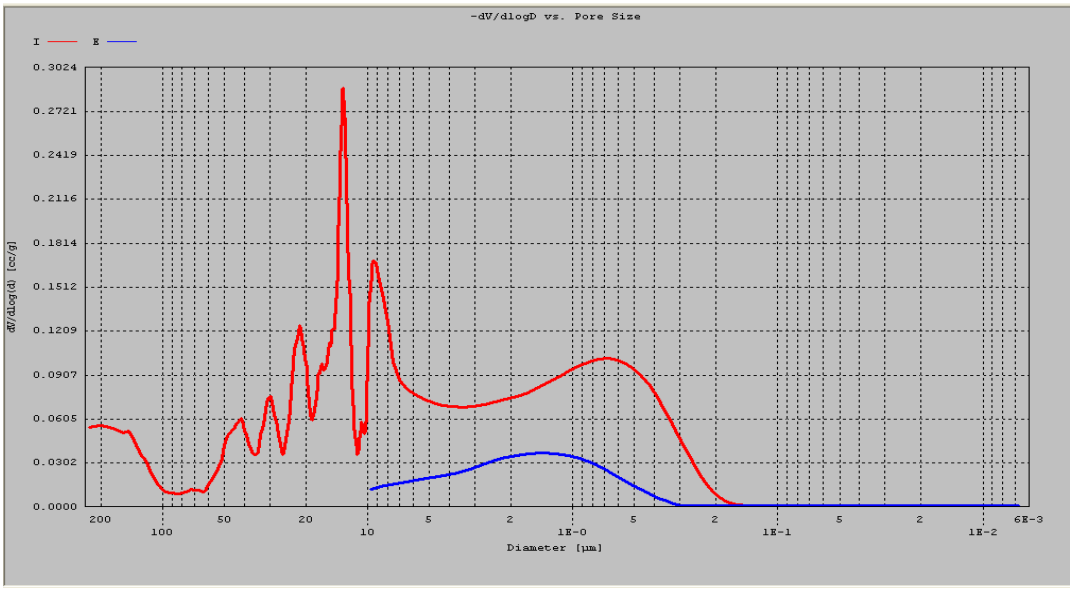

Fig. 4.28. Pore Size distribution analysis of 80% Alumina and 20% Naphthalene sample fired at 1500□C for 2 hrs

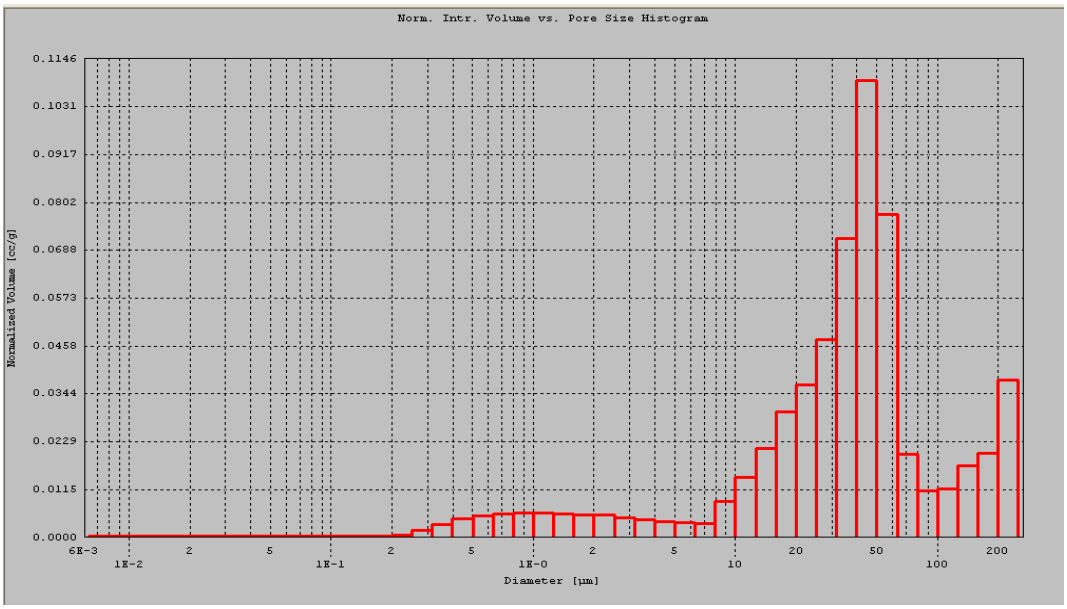

Fig. 4.29. Cumulative distribution analysis of 50% Alumina and 50% Naphthalene sample fired at 1500□C for 2 hrs

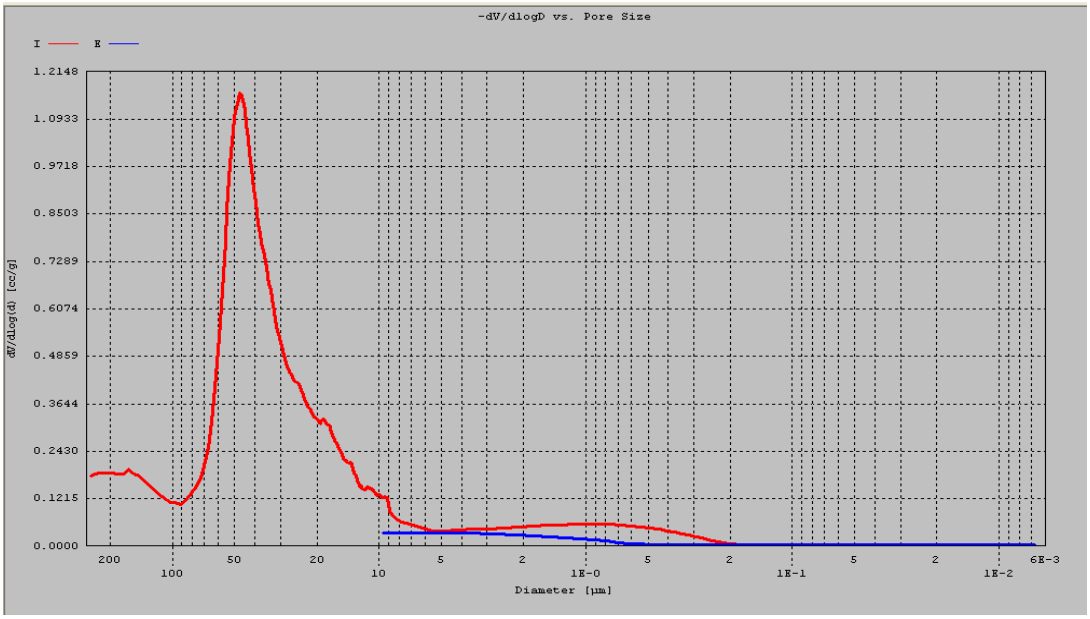

Fig. 4.30. Pore Size distribution analysis of 50% Alumina and 50% Naphthalene sample fired at 1500□C for 2 hrs

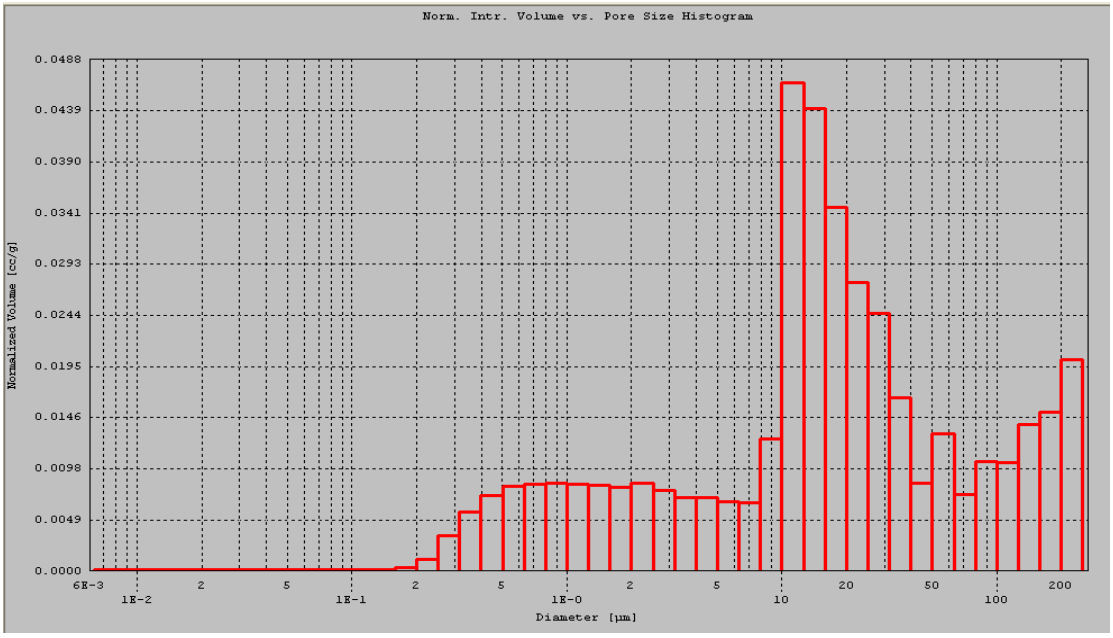

Fig. 4.31. Cumulative distribution analysis of 80% Alumina and 20% Naphthalene sample fired at 1600□C for 3 hrs

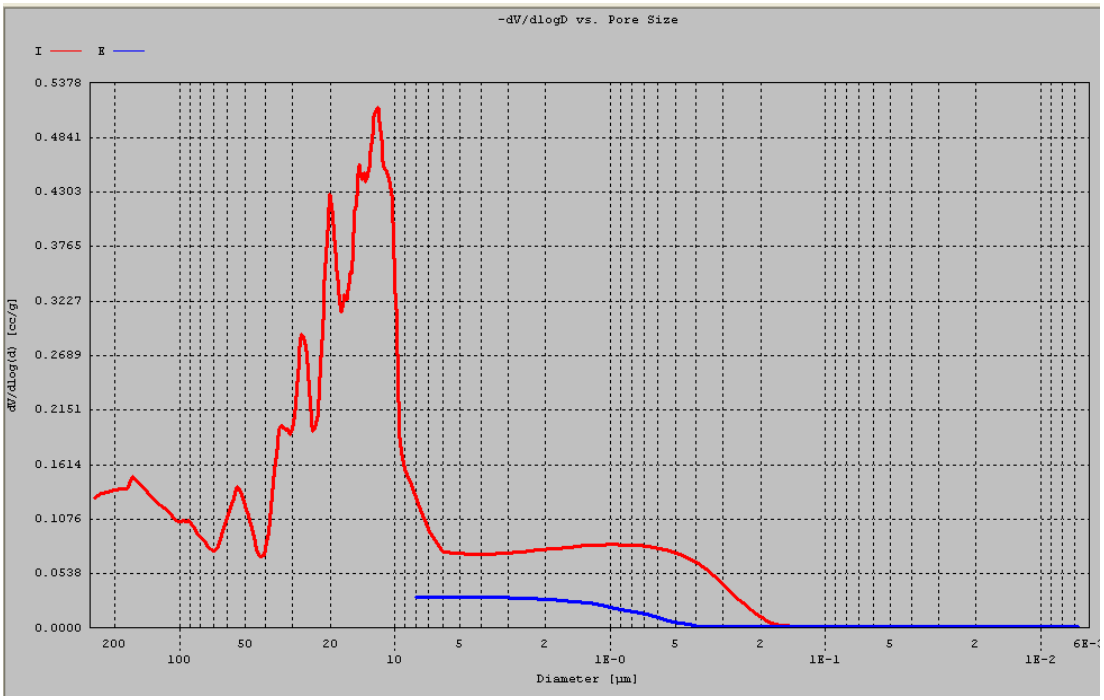

Fig. 4.32. Pore Size Distribution analysis of 80% Alumina and 20% Naphthalene sample fired at 1600□C for 3 hrs

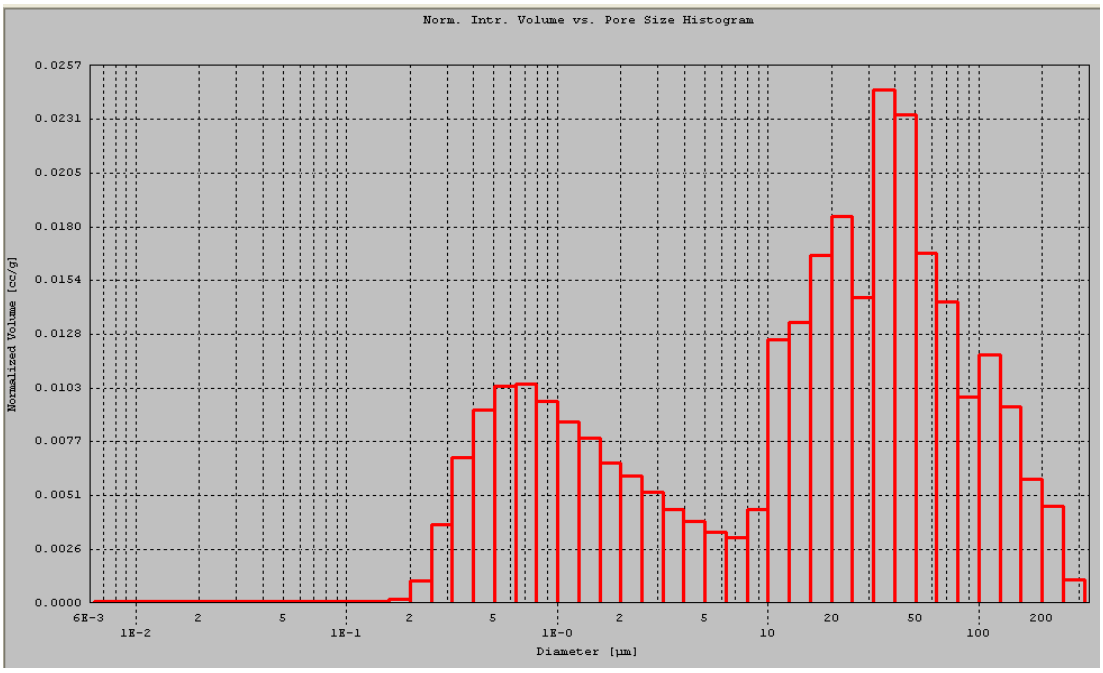

Fig. 4.33. Cumulative distribution analysis of 50% Alumina and 50% Naphthalene sample fired at 1600□C for 3 hrs

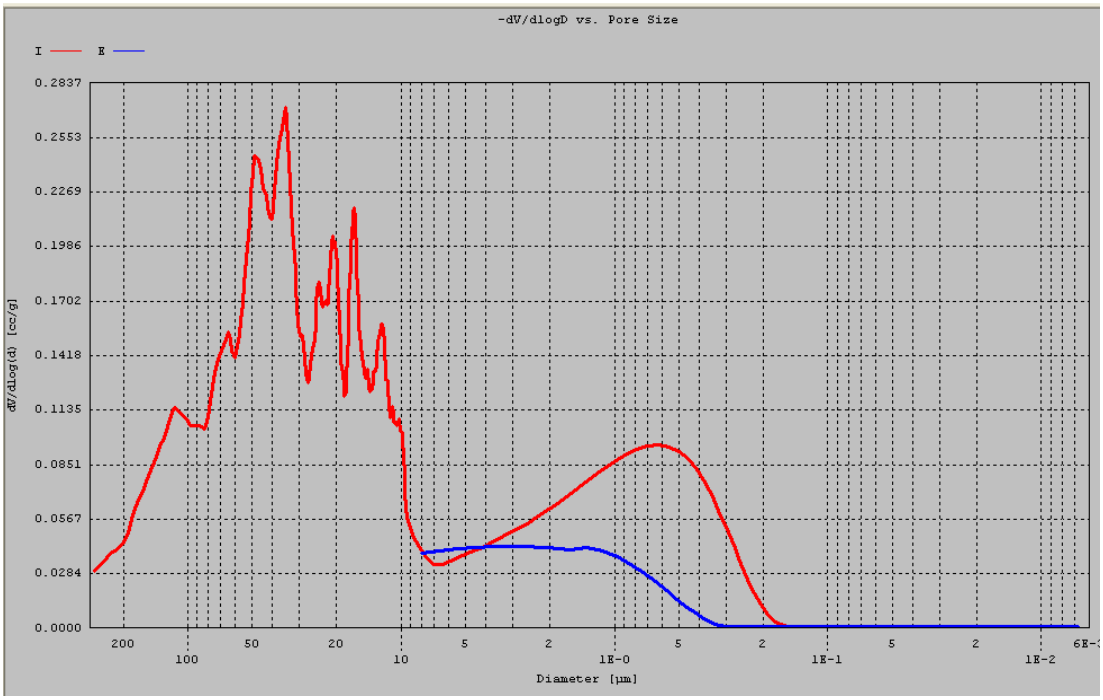

Fig. 4.34. Pore Size distribution analysis of 50% Alumina and 50% Naphthalene sample Fired at 1600□C for 3 hrs

Fig. 4.27 - 4.34 shows that with increase in sintering temperature, the pore size as well as pore size distribution shifts towards the lower pore size region. The effect is more pronounced for 80% alumina and 20% naphthalene composition.

In 50% alumina 50% naphthalene composition, the smaller pore size appears as a broad peak and although the peak does not shift much, smaller pores appear.

Thus, sintering at higher temperature for longer time period helps in pore removal and thus, the pore size distribution changes.

4.6. ***Optical Microscopy***

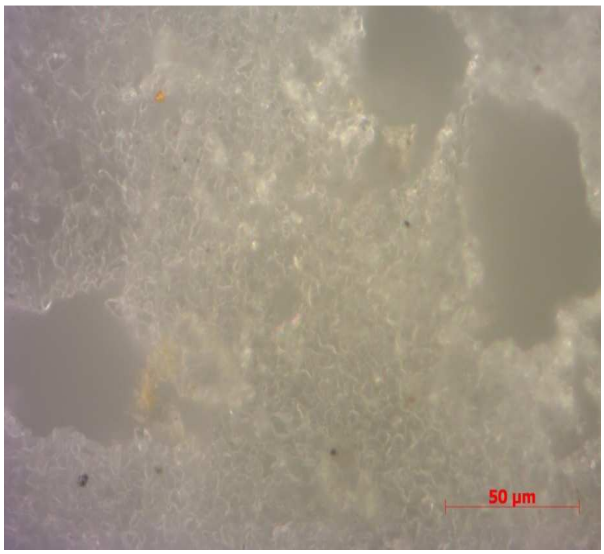

Images of pellets (80% alumina& 20% naphthalene sample) fired at1500□C for 2 hrs as seen through an an optical microscope(50x objective)

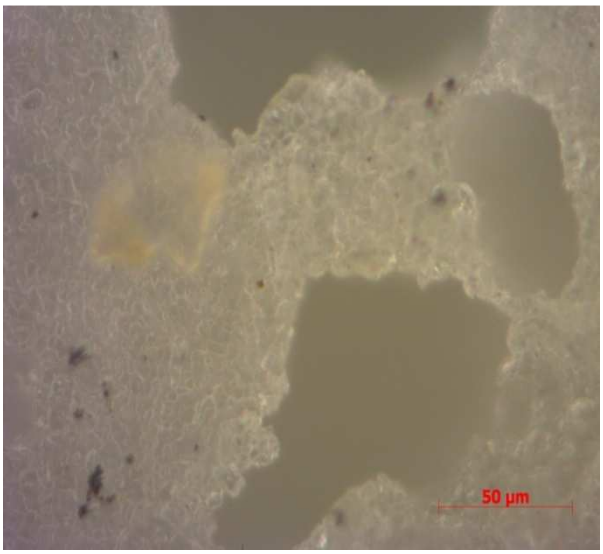

Images of pellets(70% alumina & 30% naphthalene sample) fired at at1500□C for 2 hrs as seen through optical microscope(50x objective)

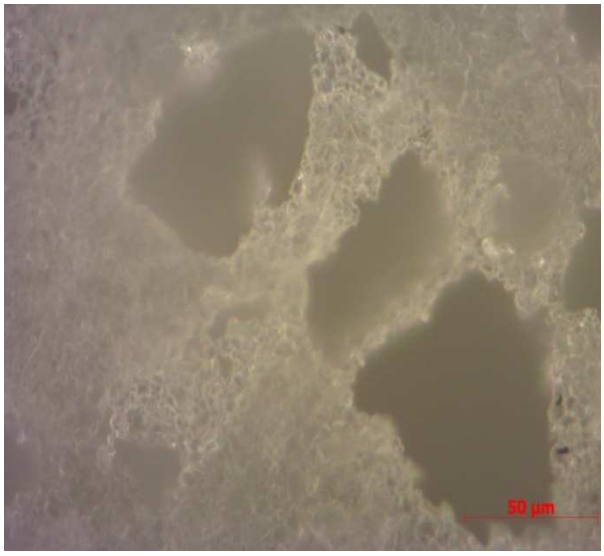

Images of pellets (60% alumina& 40% naphthalene sample) fired at1500□C for 2 hrs as seen through an an optical microscope(50x objective)

Images of pellets(50% alumina & 50% naphthalene sample) fired at at1500□C for 2 hrs as seen through optical microscope(10x objective)

Fig. 4.35. Optical Micrograph of Sintered Alumina – Naphthalene Samples

The sintered pellets were observed through an optical microscope, the number of pores observed in the sample with 50 % naphthalene was maximum. Pores were clearly visible in 50 % naphthalene sample even at 10x objective. The pore size varied from 500 nm to 300 µm.

4.7. *Scanning Electron Microscopy (SEM)*

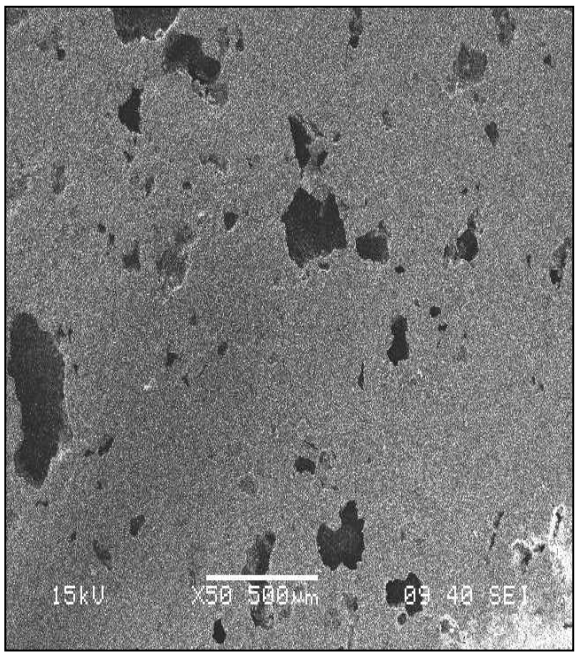

(50X MAGNIFICATION)

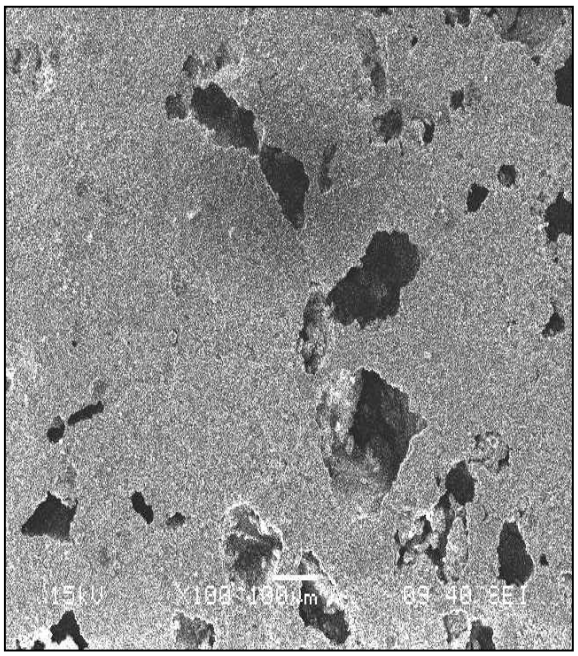

(100X MAGNIFICATION)

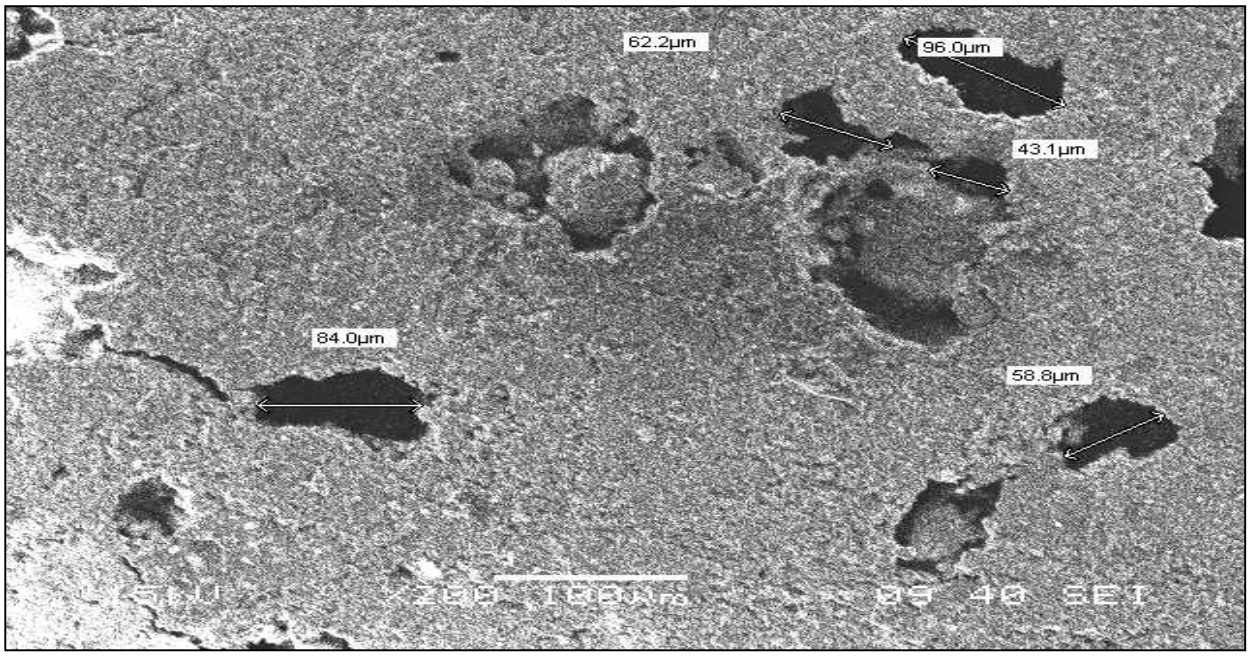

(200X MAGNIFICATION)

Fig. 4.36. SEM Images of Sintered Pellets (80% Alumina - 20% Naphthalene)

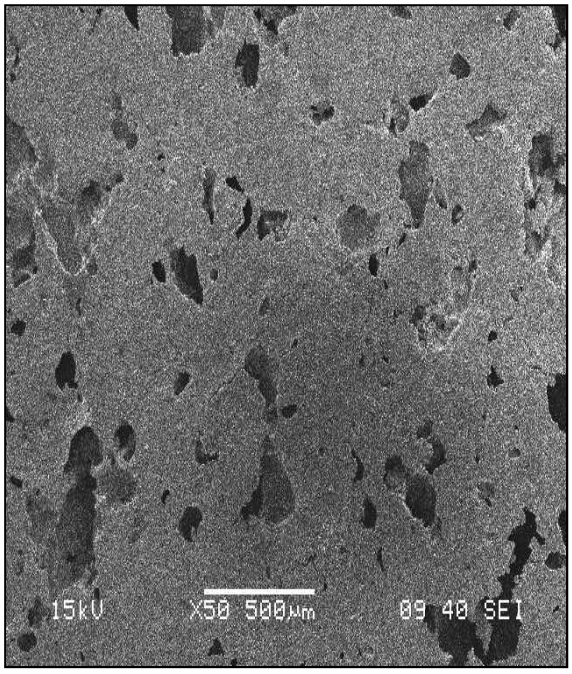

(50X MAGNIFICATION)

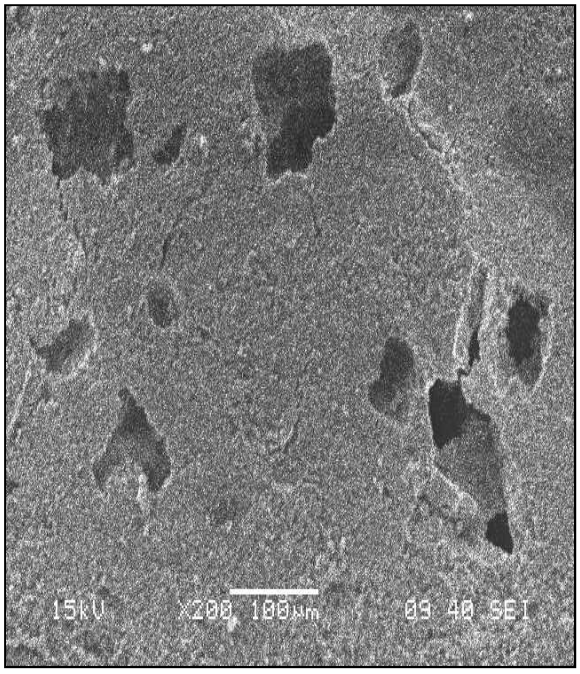

(200X MAGNIFICATION)

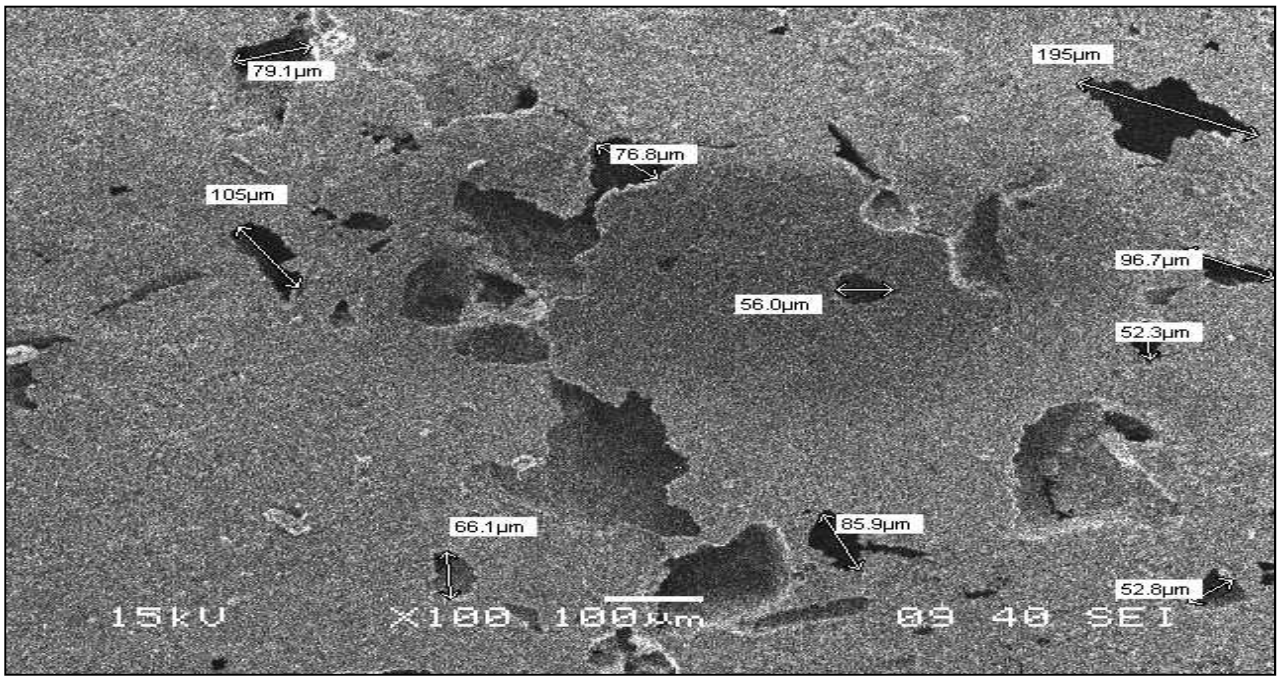

(100X MAGNIFICATION)

Fig. 4.37. SEM Images of Sintered Pellets (70% Alumina - 30% Naphthalene)

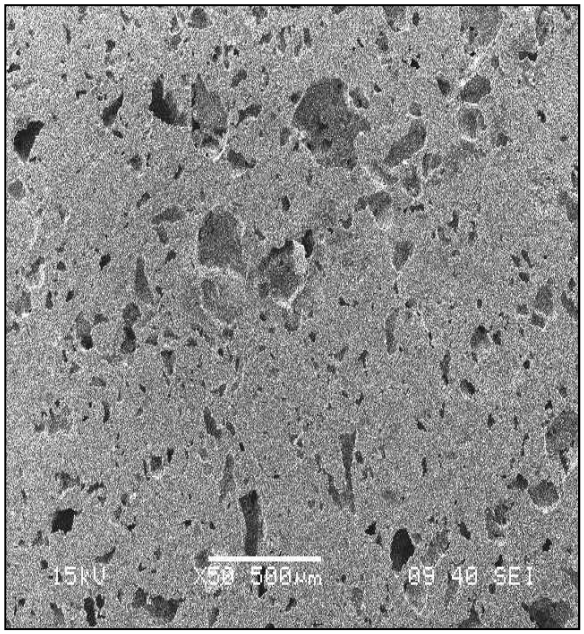

(50X MAGNIFICATION)

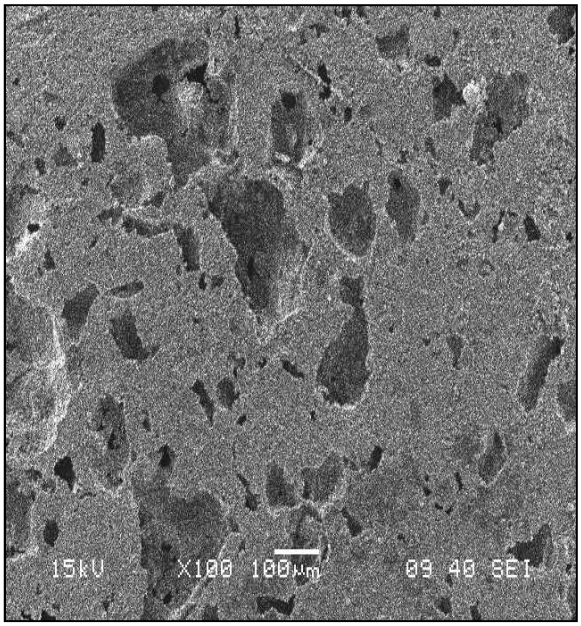

(100X MAGNIFICATION)

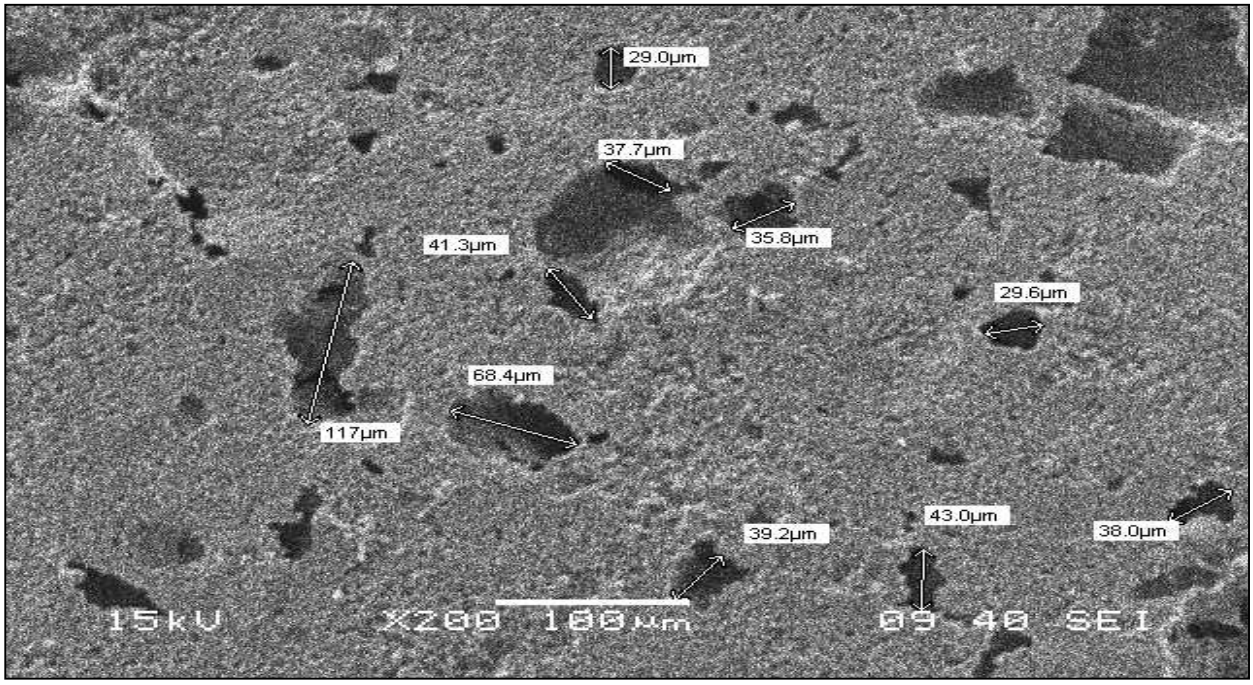

(200X MAGNIFICATION)

Fig. 4.38. SEM Images of Sintered Pellets (60% Alumina - 40% Naphthalene)

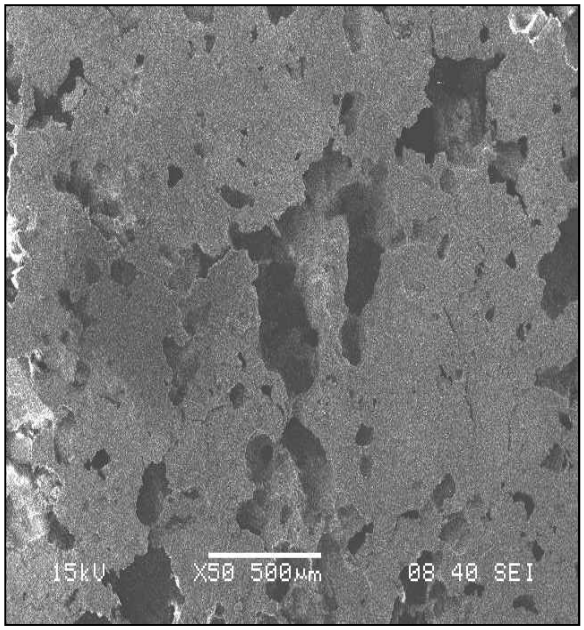

(50X MAGNIFICATION)

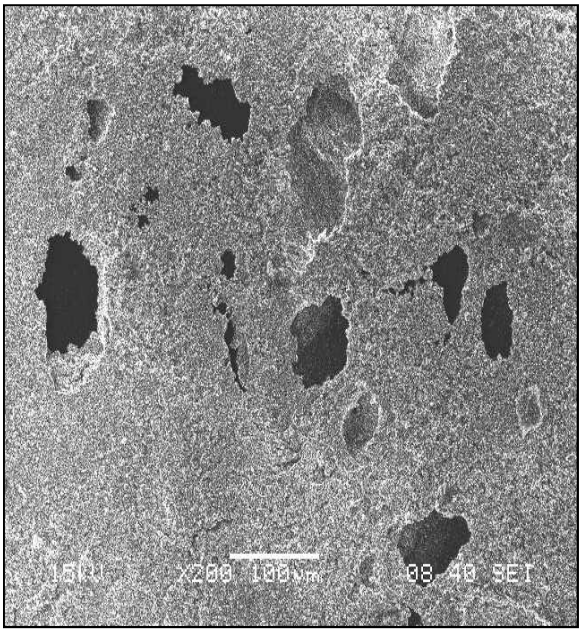

(200X MAGNIFICATION)

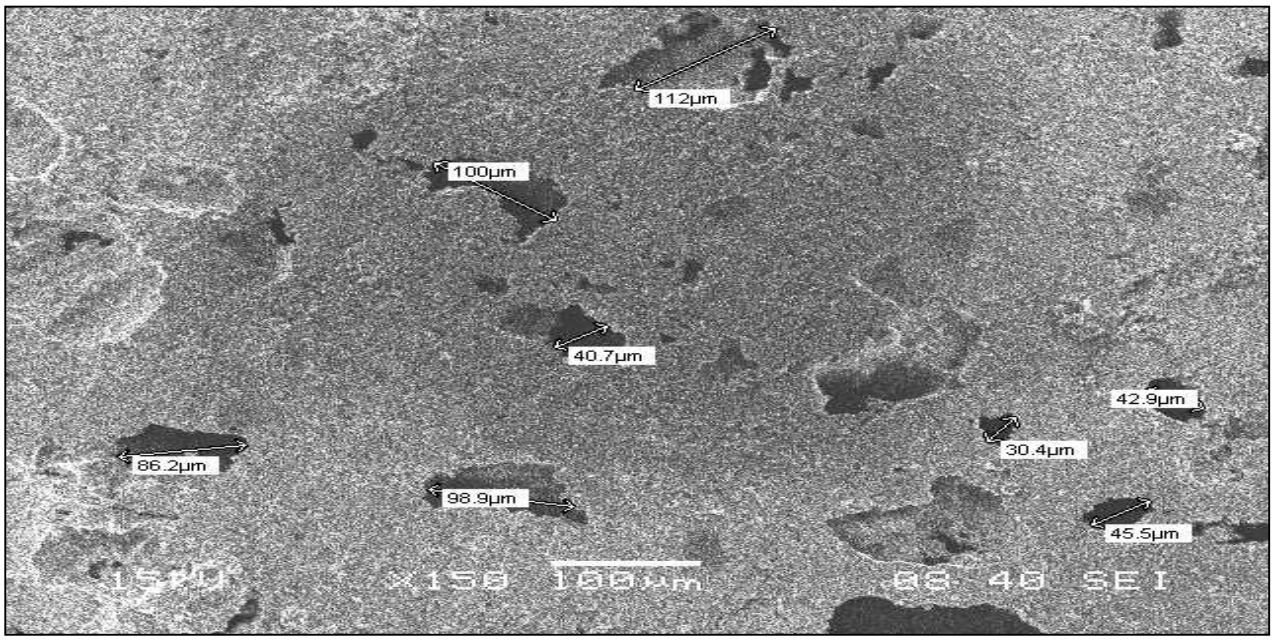

(150X MAGNIFICATION)

Fig. 4.39. SEM Images of Sintered Pellets (50% Alumina - 50% Naphthalene)

Figures 4.36 - 4.39 show SEM images of 4 different types of samples with different weight percentage of naphthalene, fired at 1600□C for 3 hours. It was seen that both macro pores (500 μm size) and micro pores (500 nm size) were interconnected. The pores were in the order of 100-300 μm. It was also seen that the pore size increased with increase in percentage of naphthalene. In samples containing higher fraction of naphthalene, some cracking of separating or intervening pore walls were also seen.

CHAPTER-5:

CONCLUSIONS

The present study dealt with the processing and characterization of alumina – naphthalene samples in which different weight percentage of naphthalene was added to create porosity in alumina samples. The green samples were sintered at 1500^{o}C, 1550^{o}C and 1600^{o}C for 2, 3 and 4 hours. The salient observations were:

1) The decomposition of naphthalene is associated with 3 endothermic peaks at 86^{o}C, 125^{o}C and 150^{o}C. DSC/TG plot of pure naphthalene show that weight loss is complete by 150^{o}C.
2) Porosity level of about 50-60% was achieved without fragmentation of samples.
3) The dilatometric curve show that pure alumina start densifying at around 1100^{o}C, while with naphthalene, the onset of densification temperature shifts to higher temperature (>1200^{o}C).
4) Sintered pellets show a decrease in CCS and flexural strength with increase in the percentage of naphthalene in the sample, which is associated with increase in porosity of samples.
5) Sintered pellets show an increase in bulk density, CCS and flexural strength and decrease in porosity & water absorption with increase in the sintering temperature & time due to decrease in the number of pores & pore size.
6) The strength vs porosity plots of sintered samples show that the strength decreases exponentially with temperature and ln (CCS) VS porosity plots show a linear fit with a negative slope.
7) Pore size distribution analysis & cumulative distribution analysis show that porosity and pore size increases with increase in the percentage of naphthalene.

8) Optical microscope shows that the numbers of pores were maximum in the alumina sample with 50% naphthalene and least in the alumina sample with 20% naphthalene.
9) SEM images show the presence of both macro and micro pores. As the porosity increased, pore walls started cracking. The pores were in the order of 100 – 300 μm. It was also seen that the size of the pores increased as the porosity increased.

REFERENCES

1) Muhammad Syamil Junid," The Fabrication of Porous Ceramic," Proceedings of 2008 student conference on research and development, Technical University of Malaysia, May 2008

2) I. Nettleship," Applications of Porous Ceramics," Key Engg. Mat. ," Vol. 122-124 (1996), pp 305-324

3) L. M. Sheppard," Porous Ceramics: Processing and Applications," Ceram. Trans. Vol. 31, pp. 3-23, 1992

4) Saggio-Woyansky, J Scott, C E Minnear, W P," Processing of Porous Ceramics," Am. Cer. Soc. Bull., Vol. 71, no. 11, pp. 1674-1682, 1992

5) Garrett Ryan, Abhay Pandit, Dimitrios Panagiotis Apatsidis, "Fabrication Methods of Porous Metals for Use in Orthopaedic Applications," Biomaterials 27 (2006) 2651–2670

6) J.F Poco, J.H Satcher Jr., L.W Hrubesh," Synthesis of High Porosity, Monolithic Alumina Aerogels," J. Non Cryst Solids, Vol. 285, Issues 1–3, June 2001, Pages 57–63

7) R. W. Rice," Porosity of Ceramics," pp. 539. Marcel Dekker Inc, New York, 1998

8) M. Scheffler, P. Colombo and Cellular Ceramics," Structure, Manufacturing, Properties and Applications," p. 645, Weinheim, Wiley-VCH, 2005

9) L. J. Gauckler, M.M. Waeber, C. Conti, and M. Jacobduliere," Ceramic Foam for Molten Metal Filtration," J. Metals, 37 [9] 47–50 (1985)

10) Sumin Zhu, Shuqiang Ding, Hong'an Xi, Ruoding Wang," Low-Temperature Fabrication of Porous SiC Ceramics by Preceramic Polymer Reaction Bonding," Mat. Lett., Vol. 59, 2005, pp 595 – 597

11) Yong Sheng Han, Jian Bao Li, Yong Jun Chen," Fabrication of bimodal porous alumina ceramics," Mat. Res. Bulln. **,** Vol. 38, Issue 2, 25 January 2003, Pages 373−379

12) Fa-Zhi Zhang, Takeaki Kato, Masayoshi Fuji, Minoru Takahashi," Gelcasting Fabrication of Porous Ceramics using a Continuous Process," J. Eur. Ceram. Soc., Vol. 26, Issues 4−5, 2006, Pages 667−671

13) Huixuan Zhang, Ye Han, Fuxiao Chen and Jiuba Wen," Fabrication of Porous Ceramic Scaffolds via Polymeric Sponge Method Using Sol-Gel Derived Strontium Doped Hydroxyapatite," App. Mech. and Mat., Vol. 117 – 119, pp 829-832, October, 2011

14) Young-Hag Koh, Hae-Won Kim and Hyoun-Ee Kim," Fabrication of Macrochannelled-Hydroxyapatite Bioceramic by a Coextrusion Process," J. Am. Ceram. Soc., 85 [10] 2578 – 80 (2002)

15) Chun-Jen Liao, Chin-Fu Chen, Jui-Hsiang Chen, Shu-Fung Chiang, Yu-Ju Lin, Ken-Yuan Chang," Fabrication of Porous Biodegradable Polymer Scaffolds Using a Solvent Particulate Leaching Method," J. Biomed. Mat. Res., Vol. 59, Issue 4, pp 676–681, 15 March 2002

16) Dean-Mo Liu," Fabrication and Characterization of Porous Hydroxyapatite Granules," Biomaterials**,** Vol. 17, Issue 20, October 1996, pp 1955−1957

17) Brad H. Jones and Timothy P. Lodge," High-Temperature Nanoporous Ceramic Monolith Prepared from a Polymeric Bicontinuous Microemulsion Template," J. Am. Chem. Soc., 2009, 131 (5), pp 1676–1677

18) J. Cao, C. R. Rambo, and H. Sieber," Preparation of Porous Alumina Ceramics by Biotemplating of Wood," J. Por. Mat. (2004), Vol. 11, Issue 3, pp 163-172

19) Ya. Guzman," Certain Principles of Formation of Porous Ceramic structures, Properties and Applications (a review)," J. Por. Mat. , No. 9, pp. 28-31, September 2003

20) E. J. A. E. Williams, J. R. G. Evans," Expanded Ceramic Foam," J. Mat. Sci., Vol. 31, 1996, pp 559-563

21) O. Lyckfeldt, J. M. F. Ferreira," Processing of Porous Ceramics by 'Starch Consolidation'," J. Eur. Ceram. Soc., Vol. 18, Issue 2, 1998, Pages 131-140

22) R. Svinka, V. Svinka, I. Zake, A. Butlers,"Influence of Some Additives on the Properties of Porous Alumina Ceramics," ISSN 1392-1231, 2009

23) Donglu Shi," Introduction to Biomaterials," Tsinghua, University Press, Pages 3-11

24) Kazutaka Kamitani, Takeo Hyodo, Yasuhiro Shimizu, and Makoto Egashira," Fabrication of Highly Porous Alumina-Based Ceramics with Connected Spaces by Employing PMMA Microspheres as a Template," Adv. Mat. Sc. and Engg., Vol. 2009 (2009), Article ID 601850, 9 pages

25) Andre´ R. Studart, Urs T. Gonzenbach, Elena Tervoort, and Ludwig J. Gauckler," Processing Routes to Macroporous Ceramics: A Review," J. Am. Ceram. Soc., 89 [6] 1771–1789 (2006)

26) M. D. M. Innocentini, P. Sepulveda, V. R. Salvini, V. C. Pandolfelli, and J. R. Coury, ''Permeability and Structure of Cellular Ceramics: A Comparison Between Two Preparation Techniques,'' J. Am. Ceram. Soc., 81 [12], 3349–52 (1998)

27) P. Sepulveda," Gelcasting Foams for Porous Ceramics,'' Am. Ceram. Soc. Bull., 76 [10] 61–5 (1997)

28) Hassna Rehman Ramay, Miqin Zhang," Preparation of Porous Hydroxyapatite Scaffolds by Combination of the Gel-Casting and Polymer Sponge Methods," Biomaterials 24 (2003) 3293–3302

29) C. R. Rambo and H. Sieber," Novel Synthetic Route to Biomorphic Al_2O_3 Ceramics,'' Adv. Mater., 17 [8] 1088 (2005)

30) P. Greil: Biomorphous Ceramics from Lignocellulosics,'' J. Eur. Ceram. Soc., 21 [2] 105–18 (2001)

31) J. Cao, C. R. Rambo, and H. Sieber," Preparation of Porous Alumina Ceramics by Biotemplating of Wood," J. Por. Mat. (2004), Vol. 11, Issue 3, pp 163-172

32) Dibyendu Chakravarty, Hayagreev Ramesh, Tata N. Rao," High Strength Porous Alumina by Spark Plasma Sintering" J. Eur. Ceram. Soc., Vol. 29, 2009,pp 1361–1369

33) P. Colombo and J. R. Hellmann," Ceramic Foams from Preceramic Polymers,'' Mater. Res. Innovations, 6 [5–6] 260–72 (2002)

34) Toshihiro Isobe, Yoshikazu Kameshima, Akira Nakajima, Kiyoshi Okada Yuji Hotta," Gas Permeability and Mechanical Properties of Porous Alumina Ceramics with Uni-Directionally Aligned Pores," J. Eur. Ceram. Soc., Vol. 27, Issue 1, 2007, Pages 53−59

35) S. M. Best, A. E. Porter, E.S. Thian, J. Huang; Bioceramics," Past, Present and for Future," J. Eur. Ceram. Soc., Vol. 28, 2008, pp 1319-1327

36) Emilie Chevalier, Dominique Chulia, Christelle Pouget, Marylene Viana," Fabrication of Porous Substrates: A Review of Processes using Pore Forming Agents in the Biomaterial Field," J. Pharm. Sc., Vol. 29, pp 1135-1154, March 2008

37) N. O. Engin, A. C. Tas," Manufacture of Porous Calcium Hydroxyapatite Bioceramics," J. Eur. Ceram. Soc., Vol. 19 (13-14), 2569-2572 (1999)

38) Dean-Mo Liu," Porous Ceramic materials: Fabrication, Characterization, Applications," Key Engg. Mat.," Vol. 115, 1995

39) Chen Ke-exin, XIAO Qun-fang, ZHOU He-ping," Preparation of Porous Hydroxyapatite Ceramics with Starch Additives," Trans. Nonferrous Met. Soc. China, Vol. 15 No.2, Apr. 2005

40) Weijiang Xue, Yang Sun, Yong Huang, Zhipeng Xie, Jialin Sun," Preparation and Properties of Porous Alumina with Highly Ordered and Unidirectional Oriented Pores by a Self-Organization Process," J. Amer. Ceram. Soc., Vol. 94, Issue 7, pages 1978–1981, July 2011

41) Carman Galassi," Processing of Porous Ceramics: Piezoelectric Materials," J. Eur. Ceram. Soc., Vol. 26, Issue 14, 2006, Pages 2951-2958

42) J. S. Reed," Principles of Ceramics Processing," 2nd edition Wiley, New York (1995).

43) P. K. Ghosh and S. Ray," Effect of Porosity and Alumina Content on the Mechanical Properties of Compocast Aluminium Alloy-Alumina Particulate Composite; J. Mat. Sc., Vol. 21, Number 5 (1986), 1667-1674